
META-REPRESENTATIONAL PREDICTIVE CODING: BIOMIMETIC SELF-SUPERVISED LEARNING

Alexander G. Ororbia
Rochester Institute of Technology
Rochester, New York, USA
ago@cs.rit.edu

Karl Friston
VERSES AI Research Lab
Los Angeles, California, USA
karl.friston@verses.ai

Rajesh P. N. Rao
University of Washington
Seattle, Washington, USA
rao@cs.washington.edu

ABSTRACT

Self-supervised learning has become an increasingly important paradigm in the domain of machine intelligence. Furthermore, evidence for self-supervised adaptation, such as contrastive formulations, has emerged in recent computational neuroscience and brain-inspired research. Nevertheless, current work on self-supervised learning relies on biologically implausible credit assignment – in the form of backpropagation of errors – and feedforward inference, typically a forward-locked pass. Predictive coding, in its mechanistic form, offers a biologically plausible means to sidestep these backprop-specific limitations. However, unsupervised predictive coding rests on learning a generative model of raw pixel input (akin to “generative AI” approaches), which entails predicting a potentially high dimensional input; on the other hand, supervised predictive coding, which learns a mapping between inputs to target labels, requires human annotation, and thus incurs the drawbacks of supervised learning. In this work, we present a scheme for self-supervised learning within a neurobiologically plausible framework that appeals to the free energy principle, constructing a new form of predictive coding that we call *meta-representational predictive coding* (MPC). MPC sidesteps the need for learning a generative model of sensory input (e.g., pixel-level features) by learning to predict *representations* of sensory input across parallel streams, resulting in an *encoder-only learning and inference scheme*. This formulation rests on active inference (in the form of sensory glimpsing) to drive the learning of representations, i.e., the representational dynamics are driven by sequences of decisions made by the model to sample informative portions of its sensorium.

Keywords Self-supervised learning · Predictive coding · Free energy optimization · Brain-inspired computing · Biological credit assignment · Biomimetic intelligence

1 Introduction

Self-supervised learning has become an increasingly important paradigm in the domain of machine intelligence [21, 35]. Furthermore, some forms of self-supervised adaptation, such as contrastive formulations — which learn how to invert the process generating data samples [120]— have emerged in computational neuroscience and brain-inspired computing [81, 90]. Nevertheless, current work on self-supervised learning (SSL) relies on biologically-implausible credit assignment – in the form of backpropagation of errors (backprop) – and inference – typically a forward-locked feedforward pass [46, 80]. A scheme that could conduct this kind of learning in a neurobiologically-plausible manner, i.e., in a backprop-free manner, would be valuable. However, current important computational and mechanistic frameworks, including most predictive coding schemes [92, 94, 75, 100], — which provide viable accounts of neurobiological inference schemes (via message passing) and credit assignment (via local plasticity rules) — are primarily formulated for learning complex generative models of raw sensory input or mapping functions between input and supervisory signals. These unsupervised and supervised forms of predictive coding, however, do not speak to a reverse perspective of neuronal inference and learning: *what might predictive coding look if it only learned a generator of latent states (an encoder only), as opposed to a generator of sensory states (a generative decoder)?* This could open the door to a form of *self-supervised predictive coding* focused on learning distributed representations of sensory stimuli without explicitly modeling high dimensional inputs.

In this work, we invert the premise of predictive processing [20, 107, 26, 15, 105] from top-down generative learning to bottom-up representation acquisition, casting the goal of free energy [32, 27] minimization as prediction in latent distributed representation spaces. To do so, we draw inspiration from how the visual system [23, 55, 69] processes stimuli through central and peripheral *streams* and eye movements such as saccades (i.e., active vision). Concretely, we frame inference and learning in the context of a predictive coding (PC) scheme that comprises an architecture of neuronal streams, some of which process central (high-resolution) views of the input while others process peripheral (low-resolution) ones. These central and peripheral streams interact by predicting the dynamics/behavior of one another. As a result, we propose a generalization of predictive coding that conducts a form of encoder-only self-supervised learning that we call **meta-representational predictive coding** (MPC). Our work makes the following contributions to biomimetic intelligence and self-supervised learning:

- We present and formulate a framework for biologically-plausible inference and credit assignment that rests on learning distributed representations of sensory input in a self-supervised manner.
- Casting self-supervised neural computation and credit assignment within and between streams results in synaptic plasticity based on local neural statistics and inference conducted in a layer-wise parallel fashion. This shows that a generative model can be learned without predicting raw sensory input (as in machine learning implementations of predictive processing) by instead predicting latent activity across visual streams; this further obviates the need for common SSL mechanisms such as the production of positive/negative examples as in contrastive learning.
- We demonstrate that MPC produces a global encoding of a sensory stimulus through an iterative sampling and processing of portions (subsets of variables) of raw input, inspired by the saccades that biological eyes enact, yielding a scalable scheme that is agnostic to the dimensionality of sensory data – the model’s representations are shown to be highly effective in several downstream supervised tasks.
- This kind of (biomimetic) PC incorporates an enactive perspective on prediction: the coordinates of where an MPC circuit is looking inform the dynamics of its constituent neuronal units, offering a stepping stone towards models of active vision and inference such as active predictive coding [93, 91].

2 Representational Predictive Coding: Cross-Circuit Latent Dynamics and Learning

Notation. In this work, we use \odot to indicate the Hadamard product (or element-wise multiplication) and \cdot to denote matrix/vector multiplication. $(\mathbf{v})^T$ is the transpose of \mathbf{v} . Matrices/vectors are depicted in bold font, e.g., matrix \mathbf{M} or vector \mathbf{v} (scalars shown in italics). \mathbf{z}_j will refer to the j th element of vector \mathbf{z} . $\langle \mathbf{a}, \mathbf{b} \rangle$ denotes vector concatenation along the column dimension; i.e., the dot or inner product. Finally, $\|\mathbf{v}\|_2$ denotes the Euclidean norm of vector \mathbf{v} . Sensory input has shape $\mathbf{x} \in \mathcal{R}^{J_0 \times 1}$ (J_0 is the number of input features), and a neural layer has shape $\mathbf{z}^\ell \in \mathcal{R}^{J_\ell \times 1}$ (J_ℓ is the number of neurons for layer ℓ). Matrix flattening (to a column vector of length equal to the product of the matrix’s number of column and rows) is denoted as $\text{Flat}()$.

2.1 Sensory Stimuli Processing: Eye Structure and Movements

As a starting point for how we structure the requisite neuronal model, we formulate its ability to selectively sample its sensorium. In terms of the model structure, we draw inspiration from the functional anatomy [118] (of animals and humans) in terms of central and peripheral vision [108, 112].¹ In visual processing [96], central and peripheral vision both play an important role. Central vision, further decomposed into foveal (extending to one degree of eccentricity from the visual field’s center containing the highest density of cone receptors with highest resolution [89, 16, 56]) and parafoveal (extending 4-5 degrees of eccentricity yet containing a high density of slightly lower-resolution rod receptors [95, 111]) vision reports higher-resolution, detailed sensory information while peripheral vision focuses on encoding coarser-grained, lower-resolution data features. Due to its higher density (and smaller receptive field size) of rods and cones, central vision is thought to be important for high spatial frequency recognition tasks [104, 68] (such as recognizing an object or face). On the other hand, peripheral vision, with the highest proportion of rods at the lowest spatial resolution, is generally viewed as important for low spatial frequency tasks that require obtaining a global gist of a scene [103, 60, 57] (or the “bigger picture” view). While it is the case that vision tends to call on central and peripheral vision differently, depending on the task [112], it is clear that these two visual streams are complementary in constructing a complete representation of the stimuli being observed

¹We regard this morphological separation underlying central/peripheral cortical anatomy as a useful biological mean-field approximation (MFA). There are many MFAs that emerge in biological self-organization and the general idea behind biological manifestations of inference-and-learning that leverage them is that the biological system will work to “repair” the falsehood(s) induced by such MFAs. Thus, a neural system, like the one we propose in this work, must work to compensate for the statistical independence assumptions between central and peripheral structures thus requiring mechanisms for passing signals between these specialized regions. This motivated our (later-described) message-passing scheme that links these structures.

at any instant. Neuroscientific evidence, in the form of brain-imaging studies, further demonstrates that orderly peripheral and central representations form/emerge in both low-level retinotopic visual areas, i.e., V1 to V4, as well in higher areas/regions that characterize the ventral temporal cortex [53, 58, 40, 38, 2] as a result of the inference and learning, evinced as visual perception or recognition (of faces, objects, or scenes). We draw inspiration from the structural organization underwriting visual perception – the visual processing afforded by foveal, parafoveal, and peripheral viewing – in constructing a neuronal circuit that (loosely) emulates this computational architecture. Furthermore, we present a predictive coding perspective [27, 100] on the accompanying neuronal circuit’s message passing and plasticity – our neuronal model’s inference and synaptic adjustments are driven by the predictions induced across foveal, parafoveal, and peripheral streams/systems (in service of optimizing free energy [27]).

In addition to structure, we draw inspiration from the oculomotor system that underwrites active vision [117, 115, 87, 72]. The ensuing visual palpation (and implicit epistemic foraging) [41] can be roughly broken down into four key movements: saccades, smooth pursuit movements, and vergence and vestibulo-ocular movements. Saccades [54, 50, 24] are rapid, ballistic (jumpy/jerky) movements which change the eye’s fixation point, the movement/shift of which ranges from smaller (in tasks such as reading) to larger saccades (examining a scene). Saccades are generally more involuntary (unconscious) than voluntarily and can, from a modeling perspective, appear to be more itinerant in nature. Smooth pursuit movement [98] entails slower movements that focus on keeping a moving stimulus on the fovea and are more voluntary in nature. Vergence movement [88] works toward aligning the fovea of each eye with targets at different distances (from the observer) whereas vestibulo-ocular movements [113] serve to stabilize the eyes relative to the observer’s niche (working to compensate for head movement, preventing the slippage of visual stimuli on the retina’s surface as the head moves).

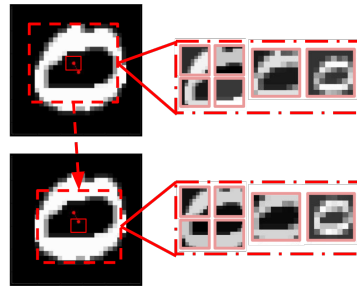


Figure 1: **Illustration of two consecutive observations of an image.** Shown is one of the digits processed by the MPC scheme over the course of two consecutive saccade-produced glimpses. On the left is the full source image with a red dashed box showing the approximate subspace sampled by the glimpse. The right panels, within the expanded dot-dashed rectangle, show how the sampled data within the dashed box on the left is converted into six input representations, i.e., four overlapping “fovea patches”, a “parafovea patch”, and a “peripheral patch”.

For the purposes of this study, we focus on saccades as the driver of our model’s information foraging, since the saccade is among the most common eye movements in humans (during waking hours) [19, 54]. In future research, we will extend our model to incorporate contextual control [99] to drive voluntary saccades and smooth pursuit. Using involuntary saccades means that our self-supervised models use an approximate of the quick, jumpy saccadic movements of biological eyes to extract partial information (“glimpses”) from the visual scene, e.g., a pixel image.

Formally, we treat an observation at time t_g , i.e., $\mathbf{o}(t_g)$ (a single static image or a frame sampled from a video; t_g marks global time in milliseconds), as a small temporary environment from which our neural models extract a fixed-length trajectory of glimpses produced as the result of randomly generated saccades (or, in future work, a motor-control policy [93]), yielding the sequence $\mathcal{S} = \left\{ (\mathbf{g}(0), \mathbf{a}(0)), (\mathbf{g}(1), \mathbf{a}(1)), \dots, (\mathbf{g}(k), \mathbf{a}(k)), \dots, (\mathbf{g}(K), \mathbf{a}(K)) \right\}$ where $\mathbf{g}(k)$ is the k -th saccade-driven “glimpse” of the sensory input, $\mathbf{a}(k) \in [-1, 1]^{2 \times 1}$ is a saccadic action or x-y coordinate vector recording the chosen center of the fixation-point of glimpse $\mathbf{g}(k)$, and K is the maximum number of steps taken.

Each glimpse vector $\mathbf{g}(k)$ is made up of several groups (pixel patches) sampled from the observation $\mathbf{o}(t_g)$. Specifically: a combination of C “foveal” views (8×8 pixel patches), F “parafoveal” views (16×16 patches), and P “peripheral” views (24×24 patches). We choose $C = 4$ (four overlapping foveal views, arranged in a 2×2 grid), $F = 1$ (one parafoveal view), and $P = 1$ (one peripheral view).² Figure 1 illustrates the result of a two-step ($K = 2$) saccade sequence over an image (of the digit zero, extracted from the MNIST database): the red dot-dashed box shows the four foveal and the single parafoveal and peripheral patches used to create $\mathbf{g}(k)$.

To obtain the final glimpse vector, all foveal, parafoveal, and peripheral views (centered around the same center-point) are first average pooled to always be the shape of $S \times S$ pixels, vectorized (i.e., flattened), and concatenated

²In the appendix, we present the results of preliminary experimentation justifying this particular arrangement of streams.

to obtain $\mathbf{g}(k) \in \mathbb{R}^{((C+F+P)*(S*S)) \times 1}$. This means that the vector $\mathbf{g}(k)$ produced by the k -th saccade is:

$$\mathbf{g}(k) = (\langle \mathbf{g}^1(k), \mathbf{g}^2(k), \dots, \mathbf{g}^v(k), \dots, \mathbf{g}^V(k) \rangle)^T \quad (1)$$

where $V = C + F + P$, brackets $\langle \cdot \rangle$ denote vector concatenation, and, specifically, indices $v = 1, 2, 3, 4$ would correspond to flattened foveal views index $v = 5$ would correspond to a flattened parafoveal view and index $v = 6$ would correspond to a flattened peripheral view. See supplement for technical details on constructing $\mathbf{g}(k)$.

The above process means that any $\mathbf{g}(k)$ is a collection of sampled sub-spaces of the observation $\mathbf{o}(t_g)$, represented in terms of several higher-resolution (smaller/close-up) views and several lower-resolution (larger/zoomed out) features. Although this scheme was designed for visual perception, a similar patch extraction process could be considered for other sensory domains, e.g., raw audio waveform representations, where relevant anatomical knowledge, e.g., the ear, spiral ganglion neurons in the cochlea, could be used to motivate the sampling scheme.

2.2 Dynamic Prediction of Latent Space Characteristics

To describe the MPC circuit model, we start with the objective that it seeks to optimize. In effect, we require predictions to be made with respect to only “parts” of its internal representations, i.e., predictions are made in portions of latent representation space. To decide what makes predictions (and what the targets of these will be), we treat the circuit as an architecture of foveal, parafoveal, and peripheral streams where each stream is specialized to receive and encode only one foveal, parafoveal, or peripheral input. Crucially, this architecture of streams, further inspired by the multi/dual-streams hypothesis [65, 36]³, must learn to predict the activity dynamics of one another; this means that each stream is continually guessing what the other streams are encoding (and each must adjust its own activities based on how wrong its guesses are). This guessing game results in a lateral, cross-stream prediction scheme, of which there are many variations that could be studied (only four are considered in this work). This type of prediction scheme enables neuronal circuits to predict the statistical properties of a latent space without making “downward” (decoder-oriented) predictions of raw sensory input. From this perspective, a successful architecture of streams would be one that seeks consistency or coherence among distributed representations.

Within an MPC architecture, each individual stream, arranged in a heterarchical or hierarchical structure, follows a variational free energy (VFE) [25, 26, 27] gradient flow that is driven by at least one other stream. In this work, we take this to mean that one stream, driven by a particular view of the sensory stimulus (at one scale/resolution, e.g., a foveal view), seeks to predict the activity values of another stream that is driven by a different yet complementary view of the same stimulus (e.g., another view but possibly at a different scale/resolution, e.g., a peripheral view). Based on the sensory views produced by the saccades in Section 2.1, the MPC architecture will consist of several “foveal” neuronal streams, “parafoveal” streams, and “peripheral” streams that seek to predict one another, resulting in a message passing scheme combining intra-stream message passing (internally-communicated mismatch signals) and inter-stream message passing (mismatches between streams). For a general architecture made of $V = C + F + P$ streams (all are assumed to have the same number of L layers and $\ell = 0$ indexes the sensory input layer), with v -th stream composed of synaptic parameters $\Theta^v = \{\mathbf{W}^{\ell,v}, \Sigma^{\ell,v}, \mathbf{A}^{\ell,v,1}, \mathbf{R}^{\ell,v,1}, \Sigma_C^{\ell,v,1}, \dots, \mathbf{A}^{\ell,v,V}, \mathbf{R}^{\ell,v,V}, \Sigma_C^{\ell,v,V}\}_{\ell=1}^L$, the resulting free energy functional for the v -th stream—which tries to predict the latent representations of any other stream ($q \neq v$) as well as possibly itself ($v = q$)—is given by:

$$\begin{aligned} \mathcal{F}_v(\Theta^v) &= \underbrace{\sum_{\ell=1}^L \sum_q \mathcal{N}(\mathbf{z}^{\ell,q}(t); \mu_C^{\ell,v,q}, \Sigma_C^{\ell,v,q})}_{\text{Cross-Representation Term}} + \underbrace{\sum_{\ell=1}^L \mathcal{N}(\mathbf{z}^{\ell,v}(t); \mu^{\ell,v}, \Sigma^{\ell,v})}_{\text{Residual Energy}} + \underbrace{\Omega(\Theta^v)}_{\text{Synaptic prior}} \quad (2) \\ &= \sum_{\ell=1}^L \sum_q \mathcal{N}(\mathbf{z}^{\ell,q}(t); \mu_C(\mathbf{z}^{\ell,v}(t), \mathbf{R}^{\ell,v,q}, \mathbf{A}^{\ell,v,q}), \Sigma_C^{\ell,v,q}) \\ &\quad + \sum_{\ell=1}^L \mathcal{N}(\mathbf{z}^{\ell,v}(t); \mu(\mathbf{z}^{\ell-1,v}(t); \mathbf{W}^{\ell,v}), \Sigma^{\ell,v}) + \sum_{p,i,j} \mathcal{N}(\Theta^v[p]_{ij}; 0, \lambda_w) \end{aligned}$$

³Note that the two-streams hypothesis specifically refers to specialized circuitry related to “what” (ventral) and “where” (dorsal) pathways. Although our architecture does not specifically implement the dorsal and ventral pathways in a neuroanatomically faithful manner, it does embody the spirit of the what-where distinction and implicit factorisation or mean-field approximation. Specifically, our model’s foveal streams acquire fine-grained information (high-resolution stroke/arc components) whereas the parafoveal and peripheral streams acquire coarse-grained information (low-resolution, object/part chunks) within which the finer-grained information is situated, i.e., the foveal visual primitives indicate what is being detected whereas the parafoveal/peripheral streams indicate where the primitives can be found in the context of the “bigger picture”.

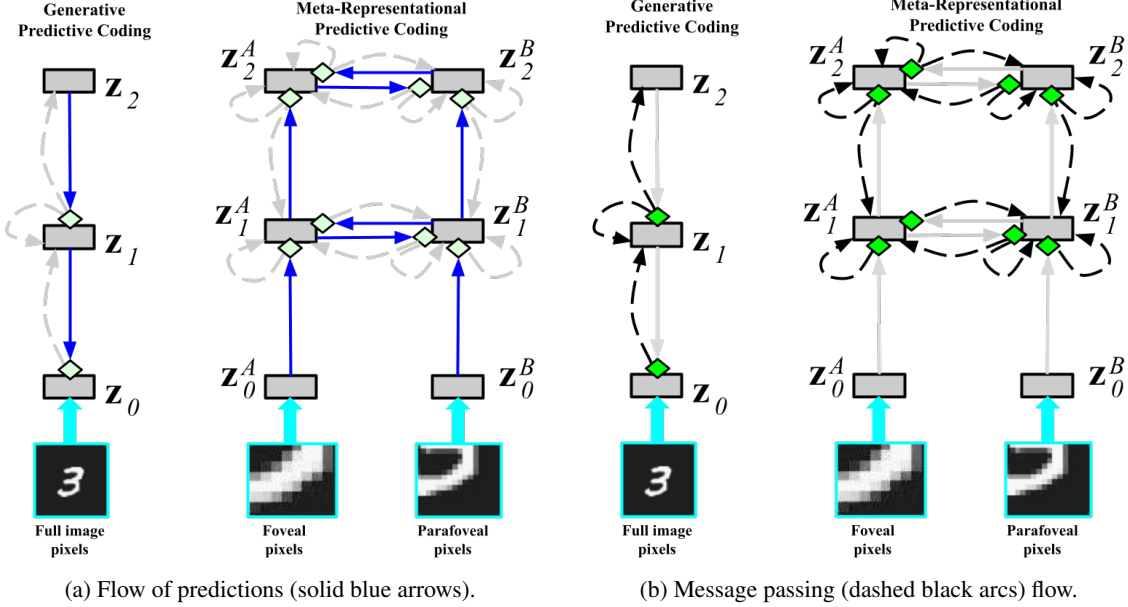


Figure 2: **Illustration of the message passing in MPC.** For generative predictive coding (GPC) and meta-representational predictive coding (MPC), depicted is: (a) the flow/directional pattern of predictions made (solid blue arrows, which indicate neuronal populations that produce a prediction) in GPC versus MPC, and (b) the flow/direction of message passing (dashed black arcs, which indicate feedback pathways that carry prediction errors) that result from GPC versus MPC prediction patterns (in sub-figure a). Solid gray boxes indicate neuronal populations encoding latent states, while green diamonds indicate populations of error neurons. Both types of PC represent the same number of latent states; the MPC shown is an architecture of two streams where stream “A” is shown processing foveal sensory information and stream “B” processes peripheral sensory information.

where the three terms can be understood as follows. The cross-representation term dictates that, at time t , any non-sensory layer $\ell > 0$ with activity $\mathbf{z}^{\ell,v}(t)$ in the v -th stream predicts the activity values $\mathbf{z}^{\ell,q}$ of the corresponding q -th target stream – the prediction connections from stream v ’s layer ℓ convey the mean $\mu_C^{\ell,v,q}$ and covariance $\Sigma_C^{\ell,v,q}$ of that layer’s prediction of $\mathbf{z}^{\ell,q}$. The residual energy term captures the fact that each individual stream is hierarchically structured, where every layer ℓ of neuronal units attempt to minimize the prediction error between its activity and the prediction of this activity by layer $\ell + 1$. The synaptic prior term is synaptic decay or, in other words, a zero-mean Gaussian prior (with standard deviation λ_w) placed over the v -th stream’s plastic synapses represented by the parameters Θ^v .⁴ Finally, for the entire MPC architecture, the “ensemble free energy” would be the combination of all of the individual stream’s VFEs: $\mathcal{F}(\Theta) = \sum_{v=1}^V \mathcal{F}_v(\Theta^v)$.

Neuronal architecture and dynamics. We next provide a mechanistic description (see Figure 2 for a depiction) of the V streams ($v \in \{1, 2, \dots, v, \dots, V\}$) that compose an MPC architecture, which optimize the VFE \mathcal{F} . Each layer of the v -th stream encodes expectations (mean values) that are parameterized as neuronal (population) activity:

$$\mu^{\ell,v} = \mu(\mathbf{z}^{\ell-1,v}(t); \mathbf{W}^{\ell,v}) = \mathbf{W}^{\ell,v} \cdot \phi^{\ell-1}(\mathbf{z}^{\ell-1,v}(t)) \quad (3)$$

where $\phi^{\ell-1}()$ denotes the element-wise nonlinearity applied to the $\ell - 1$ -th layer’s state values $\mathbf{z}^{\ell-1,v}(t)$.⁵ $\mathbf{W}^{\ell,v}$ is a matrix that contains the (intra-stream) predictive synaptic efficacies for the v -th stream. Note that the bottom (sensory) layer $\ell = 0$ of an MPC stream has no nonlinearity, i.e., $\phi^0(\mathbf{z}^{0,v}) = \mathbf{z}^{0,v}$ (the identity), and is clamped to the relevant portion of the sensory input glimpse, i.e., this means that $\mathbf{z}^{0,v}(t) = \mathbf{g}^v(k)$, where the v -th stream is provided with the v -th view of the glimpse vector $\mathbf{g}(k)$. We furthermore set the intra-stream covariance parameters to be scaled identity matrices $\Sigma^{\ell,v} = \sigma \mathbf{I}^{\ell,v}$ (where $\sigma > 0$), which simplifies VFE optimization.⁶

⁴ Θ^v is a tuple containing all of synaptic efficacy matrices for the v -th MPC stream; p retrieves the p -th synaptic parameter matrix from Θ^v , whereas i and j index a particular synapse within the p -th matrix, i.e., $\Theta^v[p]_{ij}$ returns a scalar value.

⁵Neurobiologically, in this work, we refer to values as pre- and post-synaptic depending on their relationship to the following linear algebraic transformation: $\mathbf{a} = \mathbf{W} \cdot \mathbf{b}$; \mathbf{a} contains the post-synaptic values, \mathbf{b} contains the pre-synaptic values, and \mathbf{W} contains the synaptic efficacies themselves.

⁶We remark that incorporating dynamics inherent to neuronal implementations of precision-weighting, e.g., such as the precision implementation in [109], would be useful for more complex (modeling) tasks.

In order for the v -th stream to make predictions of the q -th stream, each layer $\ell > 0$ of neurons is further equipped with lateral synaptic connections. This means that the cross-representation mean $\mu_C^{\ell,v,q}$ emitted by the v -th stream is parameterized as follows:

$$\mu_C^{\ell,v,q} = \mu_C(\mathbf{z}^{\ell,v}(t); \mathbf{R}^{\ell,v,q}, \mathbf{A}^{\ell,v,q}) = \mathbf{R}^{\ell,v,q} \cdot \phi^\ell(\mathbf{z}^{\ell,v}(t)) + \mathbf{A}^{\ell,v,q} \cdot \mathbf{a}(t) \quad (4)$$

where $\mathbf{R}^{\ell,v,q}$ contains the cross-stream prediction synapses (emitting from stream v to stream q) and $\mathbf{A}^{\ell,v,q}$ contains the action conditional, afferent synapses. $\mathbf{a}(t) \in [-1, 1]^2$ is the action taken by the MPC model at time t , specifically a two-dimensional vector encoding the chosen coordinates (positional coordinates of the sensory input relative to the MPC scheme, as described in Section 2.1 and the supplement). Furthermore, for additional simplicity, we set inter-stream covariances to be scaled identity matrices, i.e., $\Sigma_C^{\ell,v} = \sigma \mathbf{I}^{\ell,v}$ where $\sigma > 0$. Inspired by [75]—which demonstrated that lateral competition is useful for learning generative models—the activation function $\phi()$ that we chose induces a fast form of lateral competition (without requiring physical lateral synapses) in the internal layers. Specifically, we chose $\phi()$ to promote high levels of sparsity within each stream, similar in spirit to the part-whole spiking model proposed in [34]; given neuronal activities $\mathbf{z}^{\ell,v}$ as its argument, the activation $\phi(\mathbf{z}^{\ell,v})$ can be written out as follows:

$$\text{NWTA}(\mathbf{z}^{\ell,v}) = \begin{cases} z_j^{\ell,v} & z_j^{\ell,v} \in \{N_w \text{ largest elements of } \mathbf{z}^{\ell,v}\} \\ 0 & \text{otherwise} \end{cases} \quad (5)$$

which is the N -winners-take-all (NWTA) function [1] where only the N_w neurons with highest values within the layer/group $\mathbf{z}^{\ell,v}$ emit a non-zero firing rate (the rest that lose this cross-neuron competition will emit a zero). Although this winner-take-all function worked well for the experiments carried out in this study, future work would benefit by considering extensions, such as incorporating a duty-cycle [1] to promote cooperation and the sharing of firing responsibilities among neurons within a group.

Crucially, embedded within each layer $\ell > 0$ of an MPC stream is a set of prediction error neurons that compute the mismatch signals reporting how far off each layer’s predictions are from their corresponding targets. There are two kinds of error neurons, which result from the free energy functional of Equation 2, for every layer – intra-stream error units $\mathbf{e}^{\ell,v}$ and inter-stream error units $\mathbf{e}_C^{\ell,v,q}$. These two kinds of error neurons can be written down as:

$$\mathbf{e}^{\ell,v} = \mathbf{z}^{\ell,v}(t) - \mu^{\ell,v}, \quad // \text{ Intra-stream mismatch signals} \quad (6)$$

$$\mathbf{e}_C^{\ell,v,q} = \mathbf{z}^{\ell,q}(t) - \mu_C^{\ell,v,q} \quad // \text{ Inter-stream mismatch signals} \quad (7)$$

where we notice that mismatch signals will be produced as a result of either local predictions of intra-stream activity (within v), i.e., $\mu^{\ell,v}$ attempting to guess $\mathbf{z}^{\ell,v}(t)$, or inter-stream activity between v and q , i.e., $\mu_C^{\ell,v,q}$ attempting to guess $\mathbf{z}^{\ell,q}(t)$. Driven by the error neurons of Equations 6 and 7, the dynamics of the neuronal cells within each layer of an MPC stream follow the gradient flow of free energy; this flow is presented by the following (vectorized) ordinary differential equation (ODE):

$$\frac{\partial \mathcal{F}(\Theta)}{\partial \mathbf{z}^\ell(t)} = \tau_z \frac{\partial \mathbf{z}^{\ell,v}(t)}{\partial t} = -\mathbf{e}^{\ell,v} + \left(\mathbf{E}_W^{\ell,v} \cdot \mathbf{e}^{\ell+1,v} + \mathbf{E}_R^{\ell,v,q} \cdot \mathbf{e}_C^{\ell,v,q} \right) \odot \frac{\partial \phi(\mathbf{z}^{\ell,v}(t))}{\partial \mathbf{z}^{\ell,v}(t)} \quad (8)$$

where τ_z is the neural cell membrane time constant (in milliseconds; ms) and $\frac{\partial \phi(\mathbf{z}^{\ell,v})}{\partial \mathbf{z}^{\ell,v}}$ is the partial derivative of the activation function with respect to the neural state activities at t . $\mathbf{E}_W^{\ell,v}$ contains the v -th stream’s intra-stream message-passing synapses whereas $\mathbf{E}_R^{\ell,v,q}$ contain its inter-stream message-passing synapses. One more simplification—that could be applied to any MPC stream—is to set its feedback connection matrices to $\mathbf{E}_W^{\ell,v} = (\mathbf{W}^{\ell,v})^T$ and $\mathbf{E}_R^{\ell,v,q} = (\mathbf{R}^{\ell,v,q})^T$; note that these can, alternatively, be learned with Hebbian rules, as in [94, 75].

Synaptic plasticity. Learning in an MPC stream follows the gradient flow of Equation 2 and synaptic connection strengths are updated according to Hebbian plasticity rules. The intra-stream synapses $\mathbf{W}^{\ell,v}$, the inter-stream synapses $\mathbf{R}^{\ell,v,q}$, and the action-conditional afferent synapses $\mathbf{A}^{\ell,v,q}$ of any MPC stream are updated as follows:

$$\tau_w \frac{\partial \mathbf{W}^{\ell,v}}{\partial t} = -\lambda_w \mathbf{W}^{\ell,v} + \mathbf{e}^{\ell,v} \cdot (\phi(\mathbf{z}^{\ell-1,v}))^T, \quad (9)$$

$$\tau_w \frac{\partial \mathbf{R}^{\ell,v,q}}{\partial t} = -\lambda_w \mathbf{R}^{\ell,v,q} + \mathbf{e}_C^{\ell,v,q} \cdot (\phi(\mathbf{z}^{\ell,v}))^T, \quad (10)$$

$$\tau_w \frac{\partial \mathbf{A}^{\ell,v,q}}{\partial t} = -\lambda_w \mathbf{A}^{\ell,v,q} + \mathbf{e}_C^{\ell,v,q} \cdot (\mathbf{a}^{\ell,v})^T \quad (11)$$

where τ_w is a synaptic plasticity time constant (in ms) and λ_w is a synaptic decay modulation coefficient. The inference and learning steps in an MPC scheme are scheduled according to an expectation-maximization [17] (EM) like process: **1**) inference (E-step) is carried out in an MPC stream by applying Equation 8 using Euler integration,

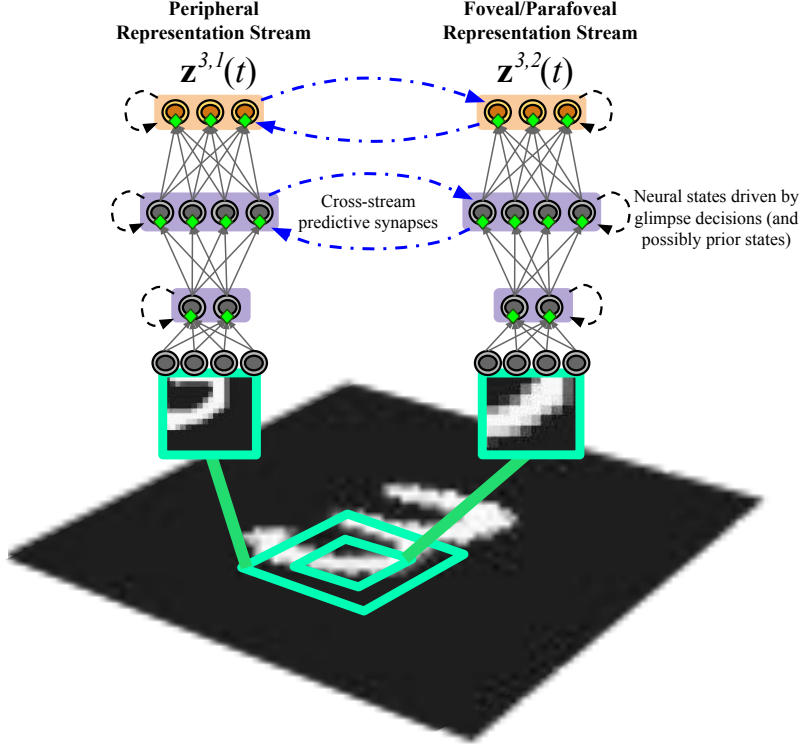


Figure 3: **Graphical depiction of a simple dual stream, MPC architecture.** A meta-representational predictive coding (MPC) architecture works by processing inputs via two or more features of the sensory input, generally at different resolutions which mimic the coarseness (acuity) of the spatial features extracted by the foveal/parafoveal and the peripheral streams of the human eye. In this image, we depict a two stream architecture, where one MPC stream produces a foveal/central representation $\mathbf{z}^{3,1}(t)$ (in its third layer) of its input at time t while another circuit produces a peripheral representation $\mathbf{z}^{3,2}(t)$ of the input (also at t). The foveal MPC stream attempts to predict the activities of the peripheral MPC circuit and *vice versa* (for the k -th glimpse at an image). Notice that all MPC streams are conditioned by the actions, i.e., normalized x-y coordinates of the fixation point of all of the foveal/parafoveal/peripheral views, taken by a saccade over the sensory input as well as possibly their prior expectation (at time $t - 1$). In this work, a fixed K -length saccade sequence is produced by randomly jumping across the sensory space, resulting in a perceptual input sampling policy. Green diamonds indicate error neuron populations, light-gray or orange circles with slightly darker colors within denote state cell populations, light gray arrows represent synaptic connections, dashed black circular arcs depict recurrent synapses, and blue dash-dotted arcs denote lateral cross-circuit prediction synapses (not shown, to improve visual clarity, are feedback synapses).

for all layers $\ell > 0$, over a stimulus window length $E = T/\Delta t$ ⁷; **2**) then synaptic learning (M-step) is performed by applying, via Euler integration, Equations 9, 10, and 11 for all layers $\ell > 0$ once. After the M-step is performed, updated synaptic matrices are constrained to have unit column Euclidean norms.

In Figure 3, we illustrate what a simple MPC architecture with $V = 2$ two streams (each with $L = 4$ layers) would look like; in this example, a single foveal stream predicts the activities (at each layer) of a single parafoveal stream and *vice versa*; hence the 'meta' aspect of the ensuing representations. Notice that, our free energy framework complements self-supervised representation learning [21] schemes, such as those that work to avoid (dimensional) collapse⁸ including information-maximization [22, 116, 5] and regularization approaches [3, 18]. Specifically, MPC espouses a meta-representational narrative for self-supervised learning; representations of data features should be able to predict one another in an internally consistent fashion. In some sense, the MPC architecture speaks to the notion that complementary views of input patterns should yield embeddings that are 'close' to one another, as in some forms of masked prediction [12, 85]. However, instead of focusing on input data, MPC operates

⁷ T is the length of stimulus presentation time for examining an input view $\mathbf{z}^{0,v}(t) = \mathbf{g}^v(k)$ and Δt is the integration time constant; both are in milliseconds (ms).

⁸Dimensional collapse refers to the case where the two branches of a dual-embedding architecture (such as a Siamese neural network [8]) degenerate to producing identical and constant output vectors. This is a degenerate outcome indicating that the model ends up learning to simply ignore the input data.

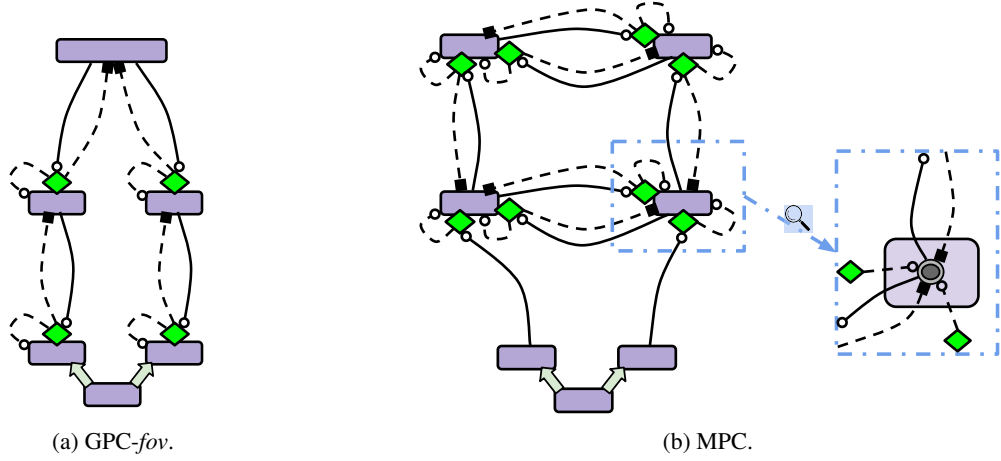


Figure 4: **Structures of generative and meta-representational predictive coding schemes.** Depicted are two proposed variants of predictive coding – a “field-of-view” form of generative predictive coding (GPC-fov) and meta-representational predictive coding (MPC) – that process the same visual scene. In this graphical example, two portions of visual input at a particular point in time are extracted (yielding a dual view, possibly containing foveal, parafoveal, or peripheral patch pixel information) by an eye movement process (represented by the pale green fat arrows), such as the involuntary saccades described in Section 2.1. Specifically, we show: (a) the proposed GPC-fov (with two neural columns) processing a dual view of the sensory input, i.e., a variant of GPC that uses the same information as our MPC models; and (b) the proposed MPC (with two neural columns or streams) processing a dual view of the sensory input. Note that solid (black) arrows with open circles denote inhibitory (predictive) synapses, dashed (black) arrows with solid squares denote a population of excitatory (message-passing) synapses, purple boxes indicate a population of neurons encoding latent states and green diamonds denote a group of error neurons for a specific layer. In the zoomed-in inset for sub-Figure 4b, we show the incoming and outgoing wired connections to a single neuron within a population.

exclusively in latent space, where parallel streams encoding input effectively learn to resonate with one another as a result of continuous prediction and message passing.

Generative predictive coding. To contrast the proposed MPC framework with standard PC [92, 75, 100] (which we will refer to as generative PC⁹; GPC), we provide a brief explication of GPC’s requisite free energy functional and its resultant dynamics. Specifically, when processing a clamped sensory input $\mathbf{z}^0(t) = \mathbf{o}(t_g)$, a GPC circuit works—under a dynamic expectation-maximization scheme—to optimize the following VFE:

$$\mathcal{F}(\Theta) = \sum_{\ell=0}^{L-1} \mathcal{N}(\mathbf{z}^\ell(t); \mu^\ell, \Sigma^\ell) + \sum_{p,i,j} \mathcal{N}(\Theta[p]_{ij}; 0, \lambda_w) \quad (12)$$

where, depending on the distribution that one assumes over sensory inputs, one can modify the above functional to use other likelihoods at specific layers, e.g., a multivariate Bernoulli distribution for $\ell = 0$ as was done in [75]. Note that the above VFE has been expressed such that it also includes the same synaptic prior used in the MPC circuit in Equation 2. Given its goal to learn how to synthesize sensory inputs, a GPC scheme usually focuses on processing and predicting the entire sensory input $\mathbf{o}(t_g)$. Much as in the MPC circuit, the expectation μ^ℓ at each layer is produced via a linear transformation, i.e., $\mu^\ell(t) = \mathbf{W}^\ell \cdot \phi(\mathbf{z}^{\ell+1}(t))$. The covariance parameters, as in the MPC model, are simplified to the scaled identity matrix $\Sigma^\ell = \sigma \mathbf{I}^\ell$ ($\sigma > 0$).

In the above VFE (Equation 12) and structure for GPC, error neurons can be represented as a subtractive difference, i.e., $\mathbf{e}^\ell = \mathbf{z}^\ell(t) - \mu^\ell(t)$, and message passing emerges as a consequence of using feedback synaptic connections in tandem with these error units. Specifically, the free energy gradient flow—that the neuronal units adhere to—is the following ODE:

$$\frac{\partial \mathcal{F}(\Theta)}{\partial \mathbf{z}^\ell(t)} = \tau_z \frac{\partial \mathbf{z}^\ell(t)}{\partial t} = -\mathbf{e}^\ell + \left(\mathbf{E}^\ell \cdot \mathbf{e}^{\ell-1} \right) \odot \frac{\partial \phi(\mathbf{z}^\ell(t))}{\partial \mathbf{z}^\ell(t)} \quad (13)$$

where $\mathbf{E}^\ell = (\mathbf{W}^\ell)^T$. Note that Equation 13 (and the VFE of Equation 12) can be further modified to incorporate additional constraints such as kurtotic priors that encourage sparsity in the latent states (we use a Laplacian prior in

⁹Even though all free energy-centric models learn probabilistic generative models, we emphasize the word “generative” to emphasize the decoder-centric nature of most standard PC models.

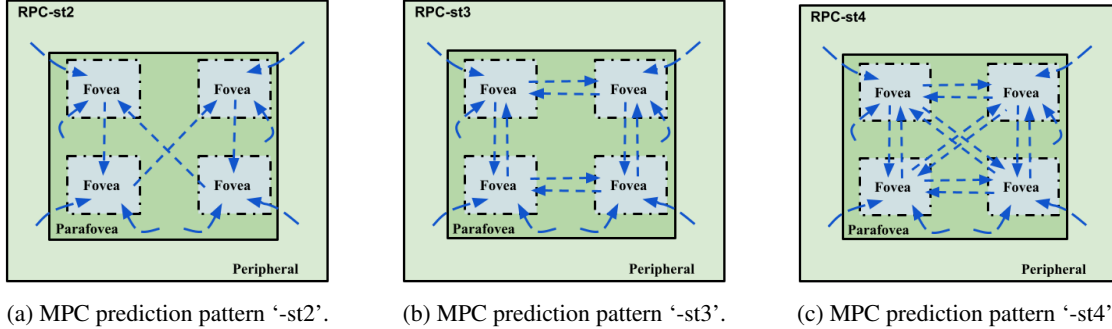


Figure 5: **Visualization of different MPC cross-circuit prediction patterns experimented with.** Above are shown three possible prediction schemes for how the individual streams interact with one another; dashed blue arrows indicate a prediction direction (blue arrow head ends on prediction target) from which error messages flow backwards. Note that each “Fovea”, “Parafovea”, and “Peripheral” box corresponds to a particular MPC stream (from a top-down view).

the GPC models studied in Section 3, to recover the modeling setups of [92] and [73]). After solving Equation 13 for $T/\Delta t$ steps (examining an observation $\mathbf{z}^0 = \mathbf{o}(t_g)$), Hebbian adjustments may be made to the synaptic weight matrices as follows:

$$\tau_w \frac{\partial \mathbf{W}^\ell}{\partial t} = -\lambda_w \mathbf{W}^\ell + \mathbf{e}^\ell \cdot (\mathbf{z}^{\ell-1})^T \quad (14)$$

where the first term (right-hand side of the equality) constitutes the controllable weight decay that emerges from the synaptic prior introduced in Equation 12; this recovers the Gaussian prior over synapses in [92]).

Note that, in this work, we further modified the above GPC model—which we named the “GPC-fov” (field-of-view GPC) model—to (iteratively) process glimpses as in MPC. In order to do so, we changed the input that the GPC model predicts to be $\mathbf{z}^0 = \mathbf{g}(k)$ and converted the GPC model’s bottom matrix \mathbf{W}^1 (or matrices $\mathbf{W}^1, \mathbf{W}^2, \dots$ up to but not including \mathbf{W}^L) closest to the input, to a block matrix with a number of blocks set equal to the number of foveal/parafoveal/peripheral streams. This means that, after every synaptic update (Equation 14), we would constrain this block structure through application of a binary mask. This variation of GPC, the “GPC-fov” model, is similar to the full patch-level model of [92] but, in this work, is a new variant that learns to generate dynamically-extracted patches of different resolutions. In Figure 4, we depict the structure of various kinds of predictive coding models we study in this work, including the classical GPC as well as the GPC-fov and MPC (both shown, for simplicity, just processing two streams of the input).

3 Experiments

Simulation setup. To demonstrate the efficacy of our MPC framework, we simulate predictive coding of two datasets of increasing complexity: **1)** the MNIST digit recognition database [52], and **2)** the Kuzushiji-MNIST (K-MNIST) character recognition database [14]. MNIST and K-MNIST contain gray-scale 28×28 images from 10 categories. MNIST contains images of handwritten digits while Kuzushiji-MNIST is a challenging drop-in replacement for MNIST, containing images depicting hand-drawn Japanese Kanji characters; in K-MNIST, each class (out of 10 classes) corresponds to the character’s modern hiragana counterpart. The only pre-processing applied to the images in these datasets was to normalize the pixel intensities to lie in the range of $[0, 1]$; note that, whenever an image patch is extracted for a patch-level models (GPC-fov and MPC circuits), we only center it (i.e., subtract the mean value of patch from the patch group of pixels). For the relevant models (GPC-fov and any MPC circuit), we process each sample pattern according to the saccade process scheme described in sub-Section 2.1.

Simulated models and baselines. We compare several circuit models (with $L = 3$ layers) in our experimental simulations: **1)** generative predictive coding (GPC) circuits that process the entire input image (the more traditional PC model), including a full-image version of the classical model in [92], a variant of this model using ReLU activations GPC-relu), and a variant of this GPC model using an NMTA activation with the number of winners scaled to match the total number of winners across all neural columns in the GPC-fov and MPC models (GPC-nmta); **2)** the GPC-fov described earlier, which processes the same sensory information as our MPC architecture, and; **3)** variants of our proposed MPC circuit. Specifically, we study four variants of our MPC model ($V = 6$ views), each with a different topological structure that dictates how the predictions are made and how the message passing is

	MNIST ACC (%)	Dec-MSE (nats)	K-MNIST ACC (%)	Dec-MSE (nats)
BP-FNN	98.04 ± 0.03	–	90.57 ± 0.11	–
JEPA [33]	95.40 ± 0.23	–	79.65 ± 0.87	–
GPC [92, 75]	91.97 ± 0.03	1.230 ± 1.088	71.09 ± 0.98	4.8005 ± 1.099
GPC- <i>relu</i>	93.78 ± 0.05	3.409 ± 0.982	78.83 ± 0.32	12.003 ± 1.332
GPC- <i>nwta</i>	95.60 ± 0.08	5.908 ± 1.002	81.99 ± 0.03	17.288 ± 1.411
GPC- <i>fov</i>	96.83 ± 0.03	7.105 ± 0.113	79.95 ± 0.09	22.679 ± 0.617
MPC-st1	97.50 ± 0.15	6.200 ± 0.987	82.22 ± 0.16	19.988 ± 0.050
MPC-st2	97.81 ± 0.02	5.761 ± 1.222	85.68 ± 0.18	20.867 ± 0.154
MPC-st3	97.74 ± 0.04	3.937 ± 0.189	85.05 ± 0.13	20.618 ± 0.021
MPC-st4	97.80 ± 0.05	4.093 ± 0.059	85.48 ± 0.02	20.706 ± 0.053

Table 1: **Generalization of different predictive coding circuits.** Measurements of generalization accuracy (ACC, in terms of %) and reconstruction decoder mean squared error (Dec-MSE, in terms of nats) of different types of predictive coding (PC) schemes (mean ± standard deviation reported for 10 trials). BP-FNN is a supervised reference model, i.e., a backprop-trained sparse feedforward neural network (with hidden ReLU activations) that directly learned a mapping between inputs and labels. GPC is a generative PC network, GPC-*fov* is generative PC reformulated to work with our saccade sensory processing scheme, and MPC is our proposed representational PC model (MPC). A dashed suffix tag refers to a particular style of cross-circuit prediction: ‘-st1’ refers to all units predict each other while ‘-st2’, ‘-st3’, and ‘-st4’ refer to variants of local, cross-stream prediction schemes (see Figure 5 for visualization of the structure of the last three prediction schemes). JEPA is the encoder-only backprop model proposed in [33] adapted to our study (to follow the same training process as well as have the same number of parameters to ensure fair comparison).

driven across streams. While we remark that many others are possible, the four cross-circuit prediction patterns that we studied (three of which are shown in 5) included:

- ‘-s1’: this is the simplest—an all-to-all structure (every column predicts all other columns and themselves);
- ‘-s2’: a single chain of local one-to-one foveal column predictions (and all parafoveal/peripheral streams predict all foveal streams as well as themselves), as in Figure 5a;
- ‘-s3’: a local two-neighbor (neighbor above or below and neighbor to the right or left) foveal column prediction scheme (and all parafoveal/peripheral streams predict all foveal streams as well as themselves), as in Figure 5b;
- ‘-s4’: all foveal streams predict all foveal streams (whereas all parafoveal/peripheral streams predict all foveal streams and themselves), as in Figure 5c.

Even though the GPC models work in an unsupervised fashion, they are all “decoder-centric” whereas all MPC circuits are “encoder-centric”. Our interest is to see if our MPC scheme offers representations as useful as these generative PC models, demonstrating that we can effectively construct encoder-centric biological models that acquire useful distributed representations of sensory input data without having to predict raw, low-level data features (e.g., pixel values).

We train all models on each database for 5 epochs with gradient ascent (using mini-batches of length 100). The learning rate of the gradient ascent optimization of parameters was tuned for each model using the validation subset of each database (we generally found the saccade-driven models preferred higher rates, while whole-image models worked better with lower rates). For any model that used the NwTA activation—the GPC-*nwta*, the GPC-*fov*, and all MPC circuits—we tuned—for each database for each model (using development data)—the number of winners in the range of $N_w = [10, 20]$ (often finding that the value of $N_w = 15$ yielded good results in general). Unless stated otherwise, all saccade-driven models, i.e., GPC-*fov* and all MPC models, used $K = 10$ saccades.

To assess each model’s efficacy, we train each under the same experimental conditions and data. Since every model is unsupervised or self-supervised, we allow each to process the data for a maximum number of epochs and adapt parameters according to their specific dynamics and plasticity mechanisms. Once a model has completed its unsupervised/self-supervised phase, we fix its synaptic connection strengths (disable its plasticity) and then allow it to process the training data, validation data, and test data once, extracting its latent representation for each data sample. If a model iteratively processes one input, we concatenated the sub-representations it produces across the K -length saccade trajectory. The resulting representations of data samples are then used in the two following down-stream analyses:

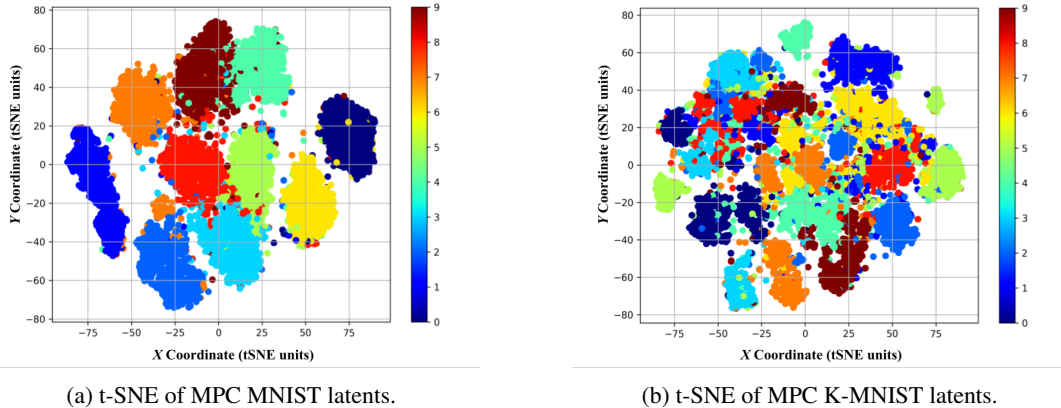


Figure 6: **Visualization of MPC-acquired latent activity codes.** t-SNE plots of the latent space induced by meta-representational predictive coding (MPC). Rate codes are shown for: (A) MPC on MNIST, and (B) MPC K-MNIST. *Note:* t-SNE coordinate units are dimensionless and are thus denoted as “tSNE units”.

- A log-linear classifier is fit to the latent codes of the training set (with validation latent codes used for hyperparameter-tuning) and then evaluated on the test-set latent codes. We report the test-set error measurements in Table 1 and compare performance against a reference backprop-trained MLP (BF-FNN).
- A single hidden-layer MLP decoder (with 1024 linear rectifier neurons in the hidden layer, trained with gradient descent and Tikhonov regularization) was retro-fit to the training-set latent codes of our MPC scheme (the MLP was also tuned using validation-set latent codes). This decoder’s reconstruction efficacy was evaluated using test-set latent codes. We report mean squared error and compare the decoder’s down-stream reconstruction against the natural reconstruction ability of the full-image GPC circuits.

3.1 Results and Analysis

Downstream usage of MPC latent codes As described before, we examined the utility of the distributed representations acquired by our MPC models in the context of downstream classification and decoding/reconstruction. The empirical results gathered from these experiments are summarized in Table 1. Specifically, we report the mean and standard deviation (over 10 uniquely-seeded experimental trials) of the test-set accuracy (ACC; higher is better) for the downstream classification probe and the test-set mean squared error (Dec-MSE; lower is better) for the downstream decoder/reconstruction probe for all models on both MNIST and K-MNIST. Observe that, although all of the self-supervised models (generative and encoder-centric) do not exceed the performance of the purely discriminative, fully-supervised BP-FNN, our proposed encoder-only MPC scheme gets quite close, with the MPC-st4 and MPC-st2 models producing generalization accuracies that are only lower by 0.21-0.23 percentage points. In terms of reconstruction, we observe that our MPC schemes facilitate the effective learning of a separate decoder, yielding decoder MSE (Dec-MSE) scores that are comparable to the powerful whole-image generative models (the GPC circuits), which themselves are trained to predict all of the pixels of the images (which are expected, in most cases, to yield the best reconstruction errors due to being specialized for reconstruction). The fact that the MPC circuits produce representations that facilitate downstream decoders that are within a few nats of the specialized GPC models is promising. In essence, Table 1 shows that MPC schemes learn, in a self-supervised fashion, distributed representations that can prove useful for both downstream classification or reconstruction. For reference, a decoder model trained with purely random

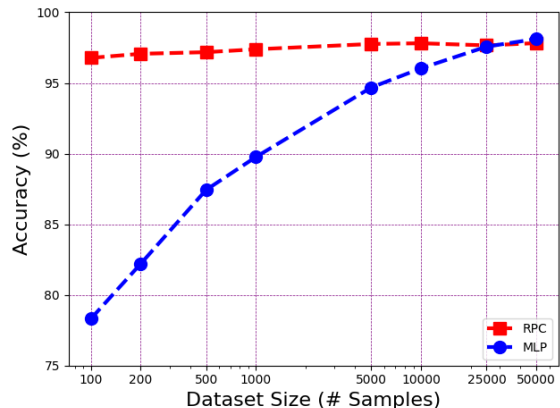


Figure 7: **Sample Efficiency on the MNIST Database.** Here, we plot test-set classification accuracy (10-trial mean values) of our best MPC against the reference BP-FNN (MLP) as a function of the number of samples used to train each model. *Note:* x-axis was plotted on a logarithmic scale to help visualise the generalization curve.

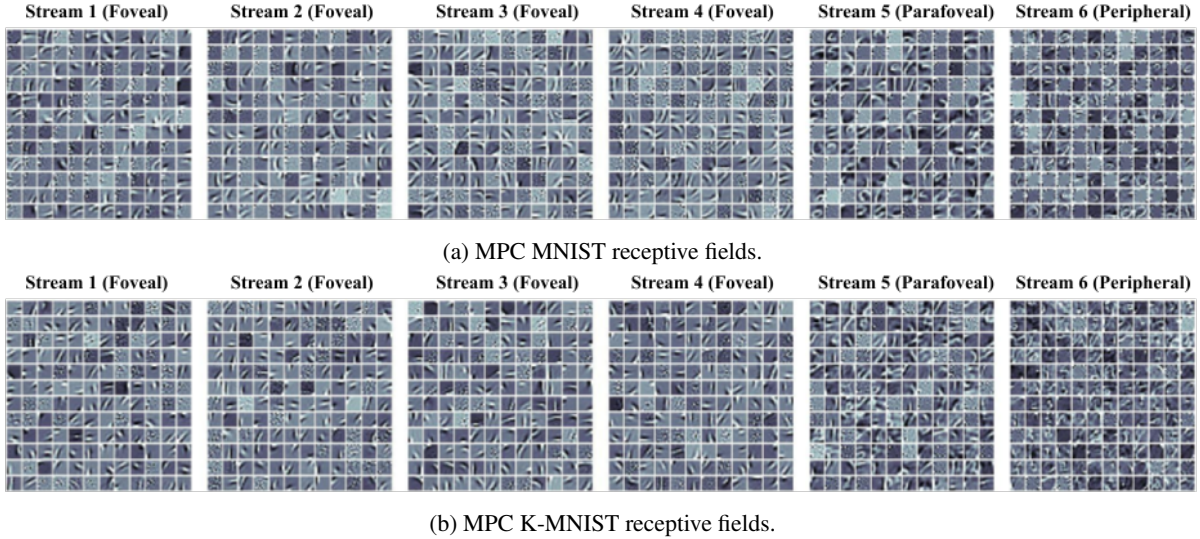


Figure 8: **Bottom-layer receptive fields acquired by an MPC scheme.** The foveal, parafoveal, and peripheral receptive fields of the bottom-most neuronal units closest to the sensory input (i.e., layer $\ell = 1$) of a meta-representational predictive coding (MPC) model, trained on MNIST patterns. Shown are the receptive fields for each of the six neural streams that make up an MPC encoder circuit.

encodings (we assigned unique random vectors to data points that were the same dimension as the concatenated set of MPC/GPC-fov representations) yields an MSE of 55.433 nats.

In Figure 7, we show the results of a small test we conducted to examine MPC’s sample efficiency on MNIST. Specifically, we re-fit MPC-st4 and the reference BP-FNN on differently-sized training datasets—dataset sizes¹⁰ included $\{100, 200, 500, 1000, 5000, 10000, 25000, 50000\}$ —and re-evaluated their generalization accuracy on the full test-set (mean values over 10 trials are plotted). Notice that as the number of available samples declines towards 100, the supervised BP-FNN’s generalization degrades significantly (as expected for a learning scheme that requires labels) whereas MPC’s downstream performance remains relatively consistent (only declining by about at most 2 percentage points). We hypothesize that MPC’s sample efficiency likely comes from the fact that it treats each data point as a sort of “mini sensorium” via its saccade-driven sampling process. This means MPC models work to extract reusable simpler features (such as strokes/arcs and object chunks) that appear to more readily/easily generalize (in MPC, the lower layers capture these atomic features whereas the upper layers produce weighted combinations of lower-level atomic features).

Qualitatively, we examined the receptive fields acquired by the neuronal units of one of our best-performing MPC circuits, the MPC-st4, by visualizing them in terms of 2D images; the results of this examination/visualization are shown in Figure 8. Note how the foveal receptive fields (the first four squares of 12×12 fields) look very similar to those acquired by classical GPC models; such as the one of [92], representing a variety of different possible strokes. These strokes are aggregated by higher-level layers of the scheme as it assembles higher-level representations of sensory input. The parafoveal and peripheral receptive fields, i.e., the last two 12×12 squares of receptive fields to the right, appear to encode either larger, more zoomed-out versions of strokes or possibly low-resolution objects/chunks of objects (digits or Kanji characters).

Beyond examining receptive fields, we visualized the relationship between the latent codes that a trained MPC circuit (MPC-st4) produced on both MNIST and K-MNIST’s test-sets. The results of this qualitative analysis used t-SNE [110] to visualize the latent codes formed with respect to the test-set samples and is presented in Figure 6. Notice that, despite never having access to the labels nor using any kind of supervisory signal, the MPC codes for MNIST tend to cluster rather well (albeit a bit noisily in some spots), yielding ten distinct major representational groupings with each corresponding to a different digit (labels were only used to color the t-SNE mapped latent code points in the t-SNE figure). For K-MNIST, we see that MPC latent codes form groupings as well but there are many more groups/clusters or “sub-groupings” than the ten identified Kanji character categories; this behavior makes sense, given that the Kanji characters are more complex and exhibit a higher degree of variety than the handwritten digits in the MNIST database.

¹⁰Samples selected from the originally training database were randomly sampled without replacement.

Assembling representations through MPC An interesting feature of the MPC model is that it represents stimuli by encoding portions of input across saccades. This means at least several glimpses of the input are needed to obtain a decent “bigger picture” encoding. To investigate how the number of glimpses affects an MPC scheme’s ability to form useful representations, we measure the performance of the model—in terms of classification accuracy—in response to the number of saccades allowed. In Figure 9, we examine the generalization of MPC (as measured in terms of downstream, test-set classification accuracy) as a function of the number of glimpses it is allowed to take (up to a maximum of 12 glimpses) when processing sensory input. Empirically, we notice that generalization improves as more glimpses are taken, up to about a little above 97.8% on average (with 10 glimpses). There is, however, a law of diminishing returns effect beyond 8-10 glimpses. This saturation might be due to the fact that enough of the sensory input was examined by the MPC circuit in order to craft a useful global representation and further glimpses added no further information. It is likely that, for more complex sensory input (natural images), more glimpses might be required to form effective global encodings. This effect motivates future work to develop a complementary motor circuit to drive the selection of the MPC sampling of the input (with a bias towards policies that entail the minimum number of saccades and that consider a better balance of representational efficiency-efficacy). This would bring our model from an action-conditioned one to a self-driven model, much in the spirit of active perception [66, 106] and selection through the framework of planning-as-inference [7, 31, 30].

Given MPC’s iterative nature, when sampling sensory input over the course of several saccades, in Figure 10, we asked what an MPC scheme is doing as it processes a sensory stimulus throughout the course of nine glimpses. Specifically, we examined two different digit patterns, i.e., a seven (in the top of Figure 10) and a zero (in the bottom of Figure 10). In addition to depicting the raw sensory glances produced by our sensory glimpsing scheme, we show the top four most activated receptive fields that each neuronal stream yields in response to the observation of a glimpse (at each time step). Notice that, for the sensory glimpse produced by each saccade, the most highly-activated foveal receptive fields capture particular, essential characteristics of the examined input, e.g., the rotation/orientation of stroke/edge of the overall digit pattern, while the most highly-activated parafoveal/peripheral fields correspond to either: **1)** capturing broader feature shapes/profiles (lower-resolution strokes and their orientations), or, **2)** engaging in a form of template matching to the most relevant low-resolution object “chunk”. In some instances, such as for the foveal streams, seemingly non-related features can appear among the more highly-activated fields, such as a stroke or edge piece that just happens to fit “within” the stimulus area of the general feature.

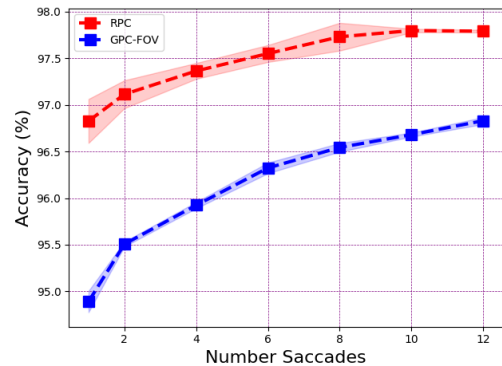


Figure 9: Analysis of Number of Saccades and Downstream MNIST Accuracy. Here, we plot our best MPC and our GPC-fov models’ performance (in terms of downstream test-set classification accuracy) as a function of the number of involuntary saccades used to construct their global representations of sensory inputs.

Limitations: As promising as our proposed MPC framework for SSL is, there are several limitations which afford avenues for future research and development. From a computational neuroscience perspective, while our MPC model designs were biomimetic, leading us to a computational architecture with foveal, parafoveal, and peripheral streams, MPC is still a loose inspiration and does not faithfully model the bio-circuitry that underlie visual hierarchies and the oculomotor system. Future effort that modifies the MPC architecture to better emulate biological details (e.g., crafting constrained layered structures that directly adhere to known neuroanatomy, operating with spikes as opposed to rate-codes, etc.) may further benefit the generalization ability of models constructed within our framing. Furthermore, it could prove fruitful to carry out neurobiological studies that ask if a cross-circuit-like prediction/message passing scheme like that of MPC affords a useful explanation of empirical neuronal responses.

From a machine intelligence point-of-view, while this work demonstrates that MPC can extract representations that facilitate promising downstream performance—demonstrating the viability of our biomimetic scheme—further experimental studies will be needed, e.g., those carried out on more complex data; including natural images and video databases. These efforts may help determine what extensions/mechanisms might be required to ensure generalization across a greater variety of (visual) sensoria/niches. It is noteworthy that our MPC framework does not rely on large batches¹¹ or batch statistics/normalization [37, 13] or negative samples as many of the modern deep learning [74, 47, 12] and neuro-mimetic schemes [44, 43, 78, 81] do. This means MPC may offer a regularization-

¹¹We used a batch size greater than one solely to speed up simulation; MPC is inherently an online learning framework.

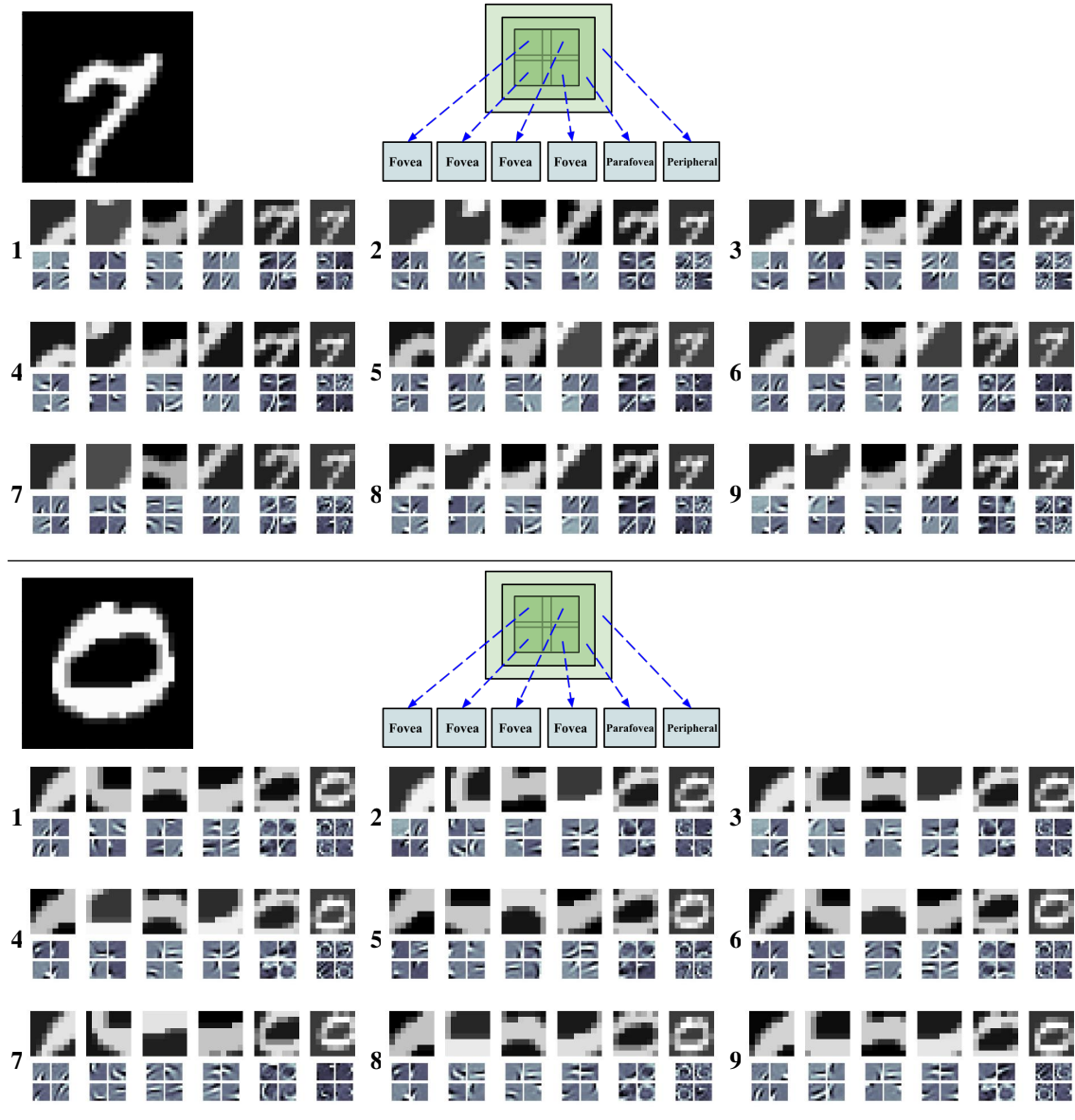


Figure 10: **A trained MPC scheme processing sensory inputs through a saccade sequence.** Shown is a trained MPC scheme iteratively processing a sensory stimulus, e.g., an image of a digit seven (top group of four rows) or a zero (bottom group of four rows), through a series of (randomly selected) saccades. Within each group of rows, which pertain to a particular sensory input digit, the first row shows a global view of the original input for reference, while the other three rows show the saccade sequence taken by the MPC scheme (the bold number indicates the saccade step k , out of nine total taken, corresponding to a particular saccade-sampled view). Within each saccade view, the first half of the image shows the sensory-level glimpses (at step k) while the bottom half contains the top four most highly activated receptive fields extracted from the MPC circuit in response to the input stimulus.

based [33, 4] SSL method that performs biologically-plausible inference and credit assignment. However, the failure cases of MPC—as well as the missing heuristics needed to scale it to be competitive with modern-day generative AI—will need to be developed. It will further be crucial to adapt and apply the analytical apparatus of self-supervised and representational learning [35], such as characterizing problems such as dimensionality collapse [48]. It is our hope that our MPC framework encourages exploration of brain-inspired and neuroscience-motivated intelligence [80, 79] in the context of SSL, a space we label *biomimetic self-supervised learning*.

Another key aspect that is missing from our framework is a mechanism for context-driven motor control¹² further inspired by machine intelligence work such as [66, 106], as it well-known that contextual task knowledge plays an important role in determining where a biological vision system looks [99]. This next generalization is further related to an implementation of the free energy principle known as active inference [31] and, since our MPC model is already action-conditional (i.e., its representations are “aware” of actions taken), our framework could yield to generalizations under active inference. In other words, it could deploy saccadic eye movements to maximize expected information gain—or epistemic affordance—of visual samples. See [28, 84, 82, 83] for worked examples.

4 Related Work

Self-supervised learning and representations. Self-supervised learning (SSL), specifically self-supervised representation learning [21] (SSRL), which can be viewed as a special case of unsupervised learning, strives to learn features or (abstract) representations of data without using supervisory annotation, e.g., labels of semantic categories. As opposed to unsupervised learning which centers around density estimation or (input data) reconstruction, SSRL relies on what are known as “pretext tasks” or artificial tasks that exploit knowledge related to a particular input modality (or modalities). Pretext SSL tasks can take a wide variety of forms, ranging from counting visual primitives in a scene [71] to in-painting [119] one part of (masked out) input using other (non-masked) portions of the input. SSRL methodology in machine intelligence research seeks to develop approaches that acquire representations (or those that learn general features) of data that facilitate strong downstream supervised learning performance without requiring time-consuming effort from human annotators (to produce the labels required by supervised learning). The chosen pretext task(s) tend to be less complex than full, raw data generative modeling, possibly yielding representations of input that are less “distracted” by noise or irrelevant data details, with many motivating cases coming from reinforcement learning research [9, 51, 59, 70].

In learning useful representations [6] or latent embeddings of input data, a wide variety of SSL/SSRL methods have been studied and developed [35]. Recent approaches, particularly those that can be labeled as “joint-embedding architectures” [5], can be broken down roughly into a few general categories: contrastive approaches, information-maximizing / regularization approaches, or those which are driven by particular heuristics [37, 97, 13]. Contrastive methods focus on constructing objectives that pull/attract embeddings of similar inputs (e.g., images) closer to one another and push embeddings of dissimilar inputs away from each other. These schemes strongly rely on either:

- **1)** an effective mining process for uncovering dissimilar images within a batch [12] or memory bank [42];
- **2)** the design of a useful synthetic process that creates out-of-distribution or negative data examples [43, 78]; or,
- **3)** a quantization/clustering scheme [10] that assigns embeddings of dissimilar data patterns to different clusters within a unit sphere.

Information-maximization SSL methods use objective functions that decorrelate and orthogonalise variable/dimension pairs within an joint-embedding of latent vectors; this is argued to (indirectly) maximize the information content of embedding vectors [5, 35]. Generally, these methods focus on either: **1)** driving the normalized cross-correlation matrix of the two embeddings (of two different, yet complementary inputs, e.g., two transformations of an image) produced by the architecture towards the identity [116, 5], or **2)** whitening and spreading out embedding vectors (of input) across the unit sphere [22]. Although MPC does not encode explicit objectives that directly maximize information, its focus on encouraging “resonant”, predictive sub-representations of different, dynamically-selected (temporally and spatially adjacent) subsets of input via a cross-stream message passing scheme brings it closest to regularization-based SSL approaches, e.g., the JEPA family [33, 4].

Biomimetic self-supervised (representation) learning. With respect to biomimetic intelligence, there have been several approaches to construct schemes that are (essentially) encoder-centric. Some approaches focus on Hebbian plasticity [39, 63, 67]; while these models have the benefit of operating with only local pre- and post-synaptic statistics—to drive various forms of associative learning—it is difficult to write down the cost/energy functionals that they are optimizing, resulting in an obscure optimization-success tracking experience.¹³ See [45] for a worked example with recurrent neural networks. More recent efforts include approaches that fall under the banner of forward-only learning [49, 79], with particular approaches such as (the unsupervised forms of) forward-forward [43] and predictive forward-forward [78] learning offering ways of conducting SSRL. Scientific inquiry along this direction has led to insights into how systems of spiking neuronal cells could engage in self-supervised forward-only learning [81, 62], building strong connections between machine learning, computational neuroscience, and

¹²Such mechanisms would prove useful for incorporating voluntary ocularmotor control as well as facilitate other types of eye movement, such as smooth pursuit or vergence.

¹³Work is ongoing for uncovering the implicit objectives that these forms of plasticity might be approximating [86, 61].

neuromorphic engineering. Nevertheless, these forms of neuro-mimetic learning inherit the same limitations as related machine learning SSL contrastive methodology, i.e., they require the generation or mining of negative samples to facilitate the proper organization of latent embeddings.

Predictive coding (PC), which is a promising biomimetic learning-and-inference scheme that has emerged from theoretical/computational neuroscience [20, 73, 92] and been continuously developed in neuroscience-inspired machine learning research [100, 80], primarily takes on the form of an auto-associative memory [102] structure (thus decoder-focused) in modeling sensoria. The goal of any unsupervised PC model is to optimize its (variational) free energy (VFE) [32, 27], leading to neuronal dynamics and message passing that follow the (gradient) flow of this VFE, where synaptic connection strengths minimize the same VFE objective, resulting in error-guided Hebbian plasticity. Most PC models are formulated as unsupervised associative memory engines (such as this work’s GPC baseline models), which predict raw sensory inputs. These models acquire their distributed representations, which constitute their underlying models-of-the-world, as a consequence of optimizing VFE [92, 27, 11, 102, 75, 101, 100]. Beyond unsupervised reconstruction, PC has been formulated for supervised learning, e.g., classification [114, 101, 76, 64], and for reinforcement learning/active inference [77]; although these PC formats often do not take on a decoder/associative memory format, they generally require annotation/human supervision to provide desired target signals or priors. This work directly recasts PC in terms of a non-auto-associative, self-supervised learning framing—meta-representational PC (MPC)—showing that it is possible, from a free energy principle perspective, to learn distributed representations of a sensorium without reconstructing raw sensory inputs. In essence, MPC entails a kind of generative learning of latent causes, guided by afferent synaptic connections that supply motor-action information to the circuit’s neuronal units (actions, in our case, being the coordinates of saccades), further elaborated by leveraging conditional independencies [29] to reproduce the computational architecture found in the visual system, e.g., central (foveal and parafoveal) and peripheral sensing, and associated parvocellular and magnocellular streams in the visual cortical hierarchy.

Active predictive coding: A recent variant of PC called active predictive coding (APC) [91, 93], which is inspired by the primacy of actions in the neocortex, utilizes a hierarchy of coupled sensory prediction and action policy modules for solving a variety of sensory-motor tasks such as active perception, learning part-whole hierarchies and spatial navigation. In APC, higher level latent sensory states and abstract actions change the lower-level state prediction function and policy function respectively according to the current task using hypernetworks or top-down modulation of lower-level networks. MPC shares with APC the emphasis on using actions (saccadic eye movements) to generate a sequence of glimpses, which are then used for self-supervised learning. While APC learns an eye movement policy to intelligently sample the scene according to the task at hand, the current implementation of MPC uses randomly generated movements. On the other hand, APC relies on prediction errors from predicting raw inputs for learning while MPC avoids input prediction and relies on prediction errors from predicting latent states across multiple visual streams. An obvious direction for future research is to combine the strengths of APC and MPC by learning hierarchical policy networks for intelligently sampling the sensorium while learning task-specific and hierarchical latent state representations via predictions across visual or more broadly, multimodal sensory streams.

5 Conclusions

In this study, we proposed a new formulation of predictive coding, *meta-representational predictive coding* (MPC), which is a biologically-motivated form of self-supervised inference and learning in service of acquiring distributed representations of sensory input. Our framework, grounded in the free energy principle, inverts the standard premise of predictive processing from one of adapting a generative model to explain raw sensory inputs to one of an encoder-centric scheme where representations of distinct data features predict each other. Empirically, our results demonstrate that casting neuronal dynamics and synaptic plasticity as message passing—induced by within and between stream prediction—offers a mechanistic explanation of how representations of sensory stimuli might emerge. In the context of visual perception, MPC is instantiated by an architecture of visual streams that are each concerned with processing foveal/parafoveal (high-resolution) or peripheral (low-resolution) sensory data features. The resulting neuronal dynamics are driven by intra- and inter-stream message passing of predictions and prediction errors.

Note the resulting framework engages with the relatively challenging problem of self-supervised learning (SSL) of representations, side-stepping the need for positive and negative data samples (as in contrastive SSL schemes) through cross visual stream prediction, showing how abstract encodings might emerge using only predictions and prediction error alone (as opposed to schemes that use similarity metrics and complementary views of data through random transformations). Our experimental simulations show that self-supervised MPC was capable of learning representations that were useful for not only downstream discriminative learning but also for downstream

reconstruction. Simulation results demonstrated that MPC was competitive with standard state-of-the-art predictive coding and backprop-trained supervised learning, even though the framework never uses label information nor does it need to predict high dimensional sensory data (e.g., pixels).

Acknowledgements

We would like to thank Viet Nguyen for writing the custom JEPa baseline used for the experiments in this paper. This research was funded in whole, or in part, by the Cisco Research Gift Award #26224 (AO). This research was funded in whole, or in part, by the Wellcome Trust [203147/Z/16/Z] (KF), the National Science Foundation (NSF) (EFRI grant no. 2223495) (RPNR), and a Frameworks grant from the Templeton World Charity Foundation (RPNR). For the purpose of Open Access, the authors have applied a CC BY public copyright license to any Author Accepted Manuscript version arising from this submission.

References

- [1] AHMAD, S., AND SCHEINKMAN, L. How can we be so dense? the benefits of using highly sparse representations. *arXiv preprint arXiv:1903.11257* (2019).
- [2] ARCARO, M. J., MCMAINS, S. A., SINGER, B. D., AND KASTNER, S. Retinotopic organization of human ventral visual cortex. *Journal of neuroscience* 29, 34 (2009), 10638–10652.
- [3] ASSRAN, M., DUVAL, Q., MISRA, I., BOJANOWSKI, P., VINCENT, P., RABBAT, M., LECUN, Y., AND BALLAS, N. Self-supervised learning from images with a joint-embedding predictive architecture. In *Proceedings of the IEEE/CVF Conference on Computer Vision and Pattern Recognition* (2023), pp. 15619–15629.
- [4] BARDES, A., GARRIDO, Q., PONCE, J., CHEN, X., RABBAT, M., LECUN, Y., ASSRAN, M., AND BALLAS, N. Revisiting feature prediction for learning visual representations from video. *arXiv preprint arXiv:2404.08471* (2024).
- [5] BARDES, A., PONCE, J., AND LECUN, Y. Vicreg: Variance-invariance-covariance regularization for self-supervised learning. *arXiv preprint arXiv:2105.04906* (2021).
- [6] BENGIO, Y., COURVILLE, A., AND VINCENT, P. Representation learning: A review and new perspectives. *IEEE transactions on pattern analysis and machine intelligence* 35, 8 (2013), 1798–1828.
- [7] BOTVINICK, M., AND TOUSSAINT, M. Planning as inference. *Trends in cognitive sciences* 16, 10 (2012), 485–488.
- [8] BROMLEY, J., GUYON, I., LECUN, Y., SÄCKINGER, E., AND SHAH, R. Signature verification using a "siamese" time delay neural network. *Advances in neural information processing systems* 6 (1993).
- [9] BURDA, Y., EDWARDS, H., STORKEY, A., AND KLIMOV, O. Exploration by random network distillation. *arXiv preprint arXiv:1810.12894* (2018).
- [10] CARON, M., BOJANOWSKI, P., JOULIN, A., AND DOUZE, M. Deep clustering for unsupervised learning of visual features. In *Proceedings of the European conference on computer vision (ECCV)* (2018), pp. 132–149.
- [11] CHALASANI, R., AND PRINCIPE, J. C. Deep predictive coding networks. *arXiv preprint arXiv:1301.3541* (2013).
- [12] CHEN, T., KORNBLITH, S., NOROUZI, M., AND HINTON, G. A simple framework for contrastive learning of visual representations. In *International conference on machine learning* (2020), PMLR, pp. 1597–1607.
- [13] CHEN, X., AND HE, K. Exploring simple siamese representation learning. In *Proceedings of the IEEE/CVF conference on computer vision and pattern recognition* (2021), pp. 15750–15758.
- [14] CLANUWAT, T., BOBER-IRIZAR, M., KITAMOTO, A., LAMB, A., YAMAMOTO, K., AND HA, D. Deep learning for classical japanese literature, 2018.
- [15] CLARK, A. *Surfing uncertainty: Prediction, action, and the embodied mind*. Oxford University Press, 2015.
- [16] CURCIO, C. A., SLOAN, K. R., KALINA, R. E., AND HENDRICKSON, A. E. Human photoreceptor topography. *Journal of comparative neurology* 292, 4 (1990), 497–523.
- [17] DEMPSTER, A. P., LAIRD, N. M., AND RUBIN, D. B. Maximum likelihood from incomplete data via the em algorithm. *Journal of the royal statistical society: series B (methodological)* 39, 1 (1977), 1–22.
- [18] DROZDOV, K., SHWARTZ-ZIV, R., AND LECUN, Y. Video representation learning with joint-embedding predictive architectures. *arXiv preprint arXiv:2412.10925* (2024).

- [19] EFRON, N. 5 - lid wiper epitheliopathy. In *Contact Lens Complications (Fourth Edition)*, N. Efron, Ed., fourth edition ed. Elsevier, Philadelphia, 2019, pp. 53–68.
- [20] ELIAS, P. Predictive coding–i. *IRE transactions on information theory* 1, 1 (1955), 16–24.
- [21] ERICSSON, L., GOUK, H., LOY, C. C., AND HOSPEDALES, T. M. Self-supervised representation learning: Introduction, advances, and challenges. *IEEE Signal Processing Magazine* 39, 3 (2022), 42–62.
- [22] ERMOLOV, A., SIAROHIN, A., SANGINETO, E., AND SEBE, N. Whitening for self-supervised representation learning. In *International conference on machine learning* (2021), PMLR, pp. 3015–3024.
- [23] FELLEMAN, D. J., AND VAN ESSEN, D. C. Distributed hierarchical processing in the primate cerebral cortex. *Cerebral cortex (New York, NY: 1991)* 1, 1 (1991), 1–47.
- [24] FINDLAY, J. M. Saccadic eye movement programming: Sensory and attentional factors. *Psychological research* 73, 2 (2009), 127–135.
- [25] FRISTON, K. A theory of cortical responses. *Philosophical Transactions of the Royal Society B: Biological Sciences* 360, 1456 (2005).
- [26] FRISTON, K. Hierarchical models in the brain. *PLoS computational biology* 4, 11 (2008), e1000211.
- [27] FRISTON, K. The free-energy principle: a unified brain theory? *Nature reviews neuroscience* 11, 2 (2010), 127–138.
- [28] FRISTON, K., ADAMS, R. A., PERRINET, L., AND BREAKSPEAR, M. Perceptions as hypotheses: saccades as experiments. *Frontiers in psychology* 3 (2012), 151.
- [29] FRISTON, K., AND BUZSÁKI, G. The functional anatomy of time: what and when in the brain. *Trends in cognitive sciences* 20, 7 (2016), 500–511.
- [30] FRISTON, K., FITZGERALD, T., RIGOLI, F., SCHWARTENBECK, P., AND PEZZULO, G. Active inference: a process theory. *Neural computation* 29, 1 (2017), 1–49.
- [31] FRISTON, K., FITZGERALD, T., RIGOLI, F., SCHWARTENBECK, P., PEZZULO, G., ET AL. Active inference and learning. *Neuroscience & Biobehavioral Reviews* 68 (2016), 862–879.
- [32] FRISTON, K., AND KIEBEL, S. Predictive coding under the free-energy principle. *Philosophical transactions of the Royal Society B: Biological sciences* 364, 1521 (2009), 1211–1221.
- [33] GARRIDO, Q., ASSRAN, M., BALLAS, N., BARDES, A., NAJMAN, L., AND LECUN, Y. Learning and leveraging world models in visual representation learning. *arXiv preprint arXiv:2403.00504* (2024).
- [34] GEBHARDT, W., AND ORORBIA, A. G. Time-integrated spike-timing-dependent-plasticity. *arXiv preprint arXiv:2407.10028* (2024).
- [35] GEIPING, J., GARRIDO, Q., FERNANDEZ, P., BAR, A., PIRSIYAVASH, H., LECUN, Y., AND GOLDBLUM, M. A cookbook of self-supervised learning. *arXiv preprint arXiv:2304.12210* (2023).
- [36] GOODALE, M. A., AND MILNER, A. D. Separate visual pathways for perception and action. *Trends in neurosciences* 15, 1 (1992), 20–25.
- [37] GRILL, J.-B., STRUB, F., ALTCHÉ, F., TALLEC, C., RICHEMOND, P., BUCHATSKAYA, E., DOERSCH, C., AVILA PIRES, B., GUO, Z., GHESLAGHI AZAR, M., ET AL. Bootstrap your own latent—a new approach to self-supervised learning. *Advances in neural information processing systems* 33 (2020), 21271–21284.
- [38] GRILL-SPECTOR, K., AND MALACH, R. The human visual cortex. *Annu. Rev. Neurosci.* 27, 1 (2004), 649–677.
- [39] GRINBERG, L., HOPFIELD, J., AND KROTOV, D. Local unsupervised learning for image analysis. *arXiv preprint arXiv:1908.08993* (2019).
- [40] HASSON, U., HAREL, M., LEVY, I., AND MALACH, R. Large-scale mirror-symmetry organization of human occipito-temporal object areas. *Neuron* 37, 6 (2003), 1027–1041.
- [41] HAYHOE, M., AND BALLARD, D. Eye movements in natural behavior. *Trends in cognitive sciences* 9, 4 (2005), 188–194.
- [42] HE, K., FAN, H., WU, Y., XIE, S., AND GIRSHICK, R. Momentum contrast for unsupervised visual representation learning. In *Proceedings of the IEEE/CVF conference on computer vision and pattern recognition* (2020), pp. 9729–9738.
- [43] HINTON, G. The forward-forward algorithm: Some preliminary investigations. *arXiv preprint arXiv:2212.13345* (2022).

- [44] HINTON, G. E. Training products of experts by minimizing contrastive divergence. *Neural computation* 14, 8 (2002), 1771–1800.
- [45] ISOMURA, T., AND FRISTON, K. Reverse-engineering neural networks to characterize their cost functions. *Neural computation* 32, 11 (2020), 2085–2121.
- [46] JADERBERG, M., CZARNECKI, W. M., OSINDERO, S., VINYALS, O., GRAVES, A., SILVER, D., AND KAVUKCUOGLU, K. Decoupled neural interfaces using synthetic gradients. In *International conference on machine learning* (2017), PMLR, pp. 1627–1635.
- [47] JAISWAL, A., BABU, A. R., ZADEH, M. Z., BANERJEE, D., AND MAKEDON, F. A survey on contrastive self-supervised learning. *Technologies* 9, 1 (2020), 2.
- [48] JING, L., VINCENT, P., LECUN, Y., AND TIAN, Y. Understanding dimensional collapse in contrastive self-supervised learning. *arXiv preprint arXiv:2110.09348* (2021).
- [49] KOHAN, A., RIETMAN, E. A., AND SIEGELMANN, H. T. Signal propagation: The framework for learning and inference in a forward pass. *IEEE Transactions on Neural Networks and Learning Systems* (2023).
- [50] KRAUZLIS, R. J. The control of voluntary eye movements: new perspectives. *The Neuroscientist* 11, 2 (2005), 124–137.
- [51] LASKIN, M., SRINIVAS, A., AND ABBEEL, P. Curl: Contrastive unsupervised representations for reinforcement learning. In *International conference on machine learning* (2020), PMLR, pp. 5639–5650.
- [52] LECUN, Y. The mnist database of handwritten digits. <http://yann.lecun.com/exdb/mnist/> (1998).
- [53] LEVY, I., HASSON, U., AVIDAN, G., HENDLER, T., AND MALACH, R. Center–periphery organization of human object areas. *Nature neuroscience* 4, 5 (2001), 533–539.
- [54] LIVERSEDGE, S. P., AND FINDLAY, J. M. Saccadic eye movements and cognition. *Trends in cognitive sciences* 4, 1 (2000), 6–14.
- [55] LIVINGSTONE, M., AND HUBEL, D. Segregation of form, color, movement, and depth: anatomy, physiology, and perception. *Science* 240, 4853 (1988), 740–749.
- [56] LOSCHKY, L., MCCONKIE, G., YANG, J., AND MILLER, M. The limits of visual resolution in natural scene viewing. *Visual Cognition* 12, 6 (2005), 1057–1092.
- [57] LOSCHKY, L. C., SETHI, A., SIMONS, D. J., PYDIMARRI, T. N., OCHS, D., AND CORBEILLE, J. L. The importance of information localization in scene gist recognition. *Journal of Experimental Psychology: Human Perception and Performance* 33, 6 (2007), 1431.
- [58] MALACH, R., LEVY, I., AND HASSON, U. The topography of high-order human object areas. *Trends in cognitive sciences* 6, 4 (2002), 176–184.
- [59] MAZZAGLIA, P., VERBELEN, T., AND DHOEDT, B. Contrastive active inference. *Advances in neural information processing systems* 34 (2021), 13870–13882.
- [60] MCCOTTER, M., GOSSELIN, F., SOWDEN, P., AND SCHYNS, P. The use of visual information in natural scenes. *Visual Cognition* 12, 6 (2005), 938–953.
- [61] MELCHIOR, J., AND WISKOTT, L. Hebbian-descent. *arXiv preprint arXiv:1905.10585* (2019).
- [62] MERKEL, C., AND ORORBIA, A. G. Contrastive learning in memristor-based neuromorphic systems. In *2024 IEEE Workshop on Signal Processing Systems (SiPS)* (2024), IEEE, pp. 171–176.
- [63] MICONI, T. Hebbian learning with gradients: Hebbian convolutional neural networks with modern deep learning frameworks. *arXiv preprint arXiv:2107.01729* (2021).
- [64] MILLIDGE, B., TSCHANTZ, A., AND BUCKLEY, C. L. Predictive coding approximates backprop along arbitrary computation graphs. *Neural Computation* 34, 6 (2022), 1329–1368.
- [65] MISHKIN, M., AND UNGERLEIDER, L. G. Contribution of striate inputs to the visuospatial functions of parieto-occipital cortex in monkeys. *Behavioural brain research* 6, 1 (1982), 57–77.
- [66] MNIH, V., HEES, N., GRAVES, A., ET AL. Recurrent models of visual attention. *Advances in neural information processing systems* 27 (2014).
- [67] MORAITIS, T., TOICHKIN, D., JOURNÉ, A., CHUA, Y., AND GUO, Q. Softhebb: Bayesian inference in unsupervised hebbian soft winner-take-all networks. *Neuromorphic Computing and Engineering* 2, 4 (2022), 044017.

- [68] MUSEL, B., BORDIER, C., DOJAT, M., PICHAT, C., CHOKRON, S., LE BAS, J.-F., AND PEYRIN, C. Retinotopic and lateralized processing of spatial frequencies in human visual cortex during scene categorization. *Journal of Cognitive Neuroscience* 25, 8 (2013), 1315–1331.
- [69] NEALEY, T. A., AND MAUNSELL, J. Magnocellular and parvocellular contributions to the responses of neurons in macaque striate cortex. *Journal of Neuroscience* 14, 4 (1994), 2069–2079.
- [70] NGUYEN, V. D., YANG, Z., BUCKLEY, C. L., AND ORORBIA, A. R-aif: Solving sparse-reward robotic tasks from pixels with active inference and world models. *arXiv preprint arXiv:2409.14216* (2024).
- [71] NOROOZI, M., PIRSIYAVASH, H., AND FAVARO, P. Representation learning by learning to count. In *Proceedings of the IEEE international conference on computer vision* (2017), pp. 5898–5906.
- [72] OGNIBENE, D., AND BALDASSARE, G. Ecological active vision: four bioinspired principles to integrate bottom–up and adaptive top–down attention tested with a simple camera-arm robot. *IEEE transactions on autonomous mental development* 7, 1 (2014), 3–25.
- [73] OLSHAUSEN, B. A., AND FIELD, D. J. Sparse coding with an overcomplete basis set: A strategy employed by v1? *Vision research* 37, 23 (1997), 3311–3325.
- [74] OORD, A. V. D., LI, Y., AND VINYALS, O. Representation learning with contrastive predictive coding. *arXiv preprint arXiv:1807.03748* (2018).
- [75] ORORBIA, A., AND KIFER, D. The neural coding framework for learning generative models. *Nature communications* 13, 1 (2022), 2064.
- [76] ORORBIA, A., AND MALI, A. Convolutional neural generative coding: Scaling predictive coding to natural images. *arXiv preprint arXiv:2211.12047* (2022).
- [77] ORORBIA, A., AND MALI, A. Active predictive coding: Brain-inspired reinforcement learning for sparse reward robotic control problems. In *2023 IEEE International Conference on Robotics and Automation (ICRA)* (2023), IEEE, pp. 3015–3021.
- [78] ORORBIA, A., AND MALI, A. The predictive forward-forward algorithm. *arXiv preprint arXiv:2301.01452* (2023).
- [79] ORORBIA, A., MALI, A., KOHAN, A., MILLIDGE, B., AND SALVATORI, T. A review of neuroscience-inspired machine learning. *arXiv preprint arXiv:2403.18929* (2024).
- [80] ORORBIA, A. G. Brain-inspired machine intelligence: A survey of neurobiologically-plausible credit assignment. *arXiv preprint arXiv:2312.09257* (2023).
- [81] ORORBIA, A. G. Contrastive signal–dependent plasticity: Self-supervised learning in spiking neural circuits. *Science Advances* 10, 43 (2024), eadn6076.
- [82] PARR, T., AND FRISTON, K. J. The active construction of the visual world. *Neuropsychologia* 104 (2017), 92–101.
- [83] PARR, T., AND FRISTON, K. J. Uncertainty, epistemics and active inference. *Journal of the Royal Society Interface* 14, 136 (2017), 20170376.
- [84] PARR, T., AND FRISTON, K. J. Working memory, attention, and salience in active inference. *Scientific reports* 7, 1 (2017), 14678.
- [85] PATHAK, D., KRAHENBUHL, P., DONAHUE, J., DARRELL, T., AND EFROS, A. A. Context encoders: Feature learning by inpainting. In *Proceedings of the IEEE conference on computer vision and pattern recognition* (2016), pp. 2536–2544.
- [86] PEHLEVAN, C., SENGUPTA, A. M., AND CHKLOVSKII, D. B. Why do similarity matching objectives lead to hebbian/anti-hebbian networks? *Neural computation* 30, 1 (2017), 84–124.
- [87] PERRINET, L. U., ADAMS, R. A., AND FRISTON, K. J. Active inference, eye movements and oculomotor delays. *Biological cybernetics* 108 (2014), 777–801.
- [88] PIERROT-DESEILLIGNY, C., MILEA, D., AND MÜRI, R. M. Eye movement control by the cerebral cortex. *Current opinion in neurology* 17, 1 (2004), 17–25.
- [89] POLYAK, S. L. *The retina*. Univ. Chicago Press, 1941.
- [90] PRINCE, J. S., ALVAREZ, G. A., AND KONKLE, T. Contrastive learning explains the emergence and function of visual category-selective regions. *Science Advances* 10, 39 (2024), ead11776.
- [91] RAO, R. P. A sensory–motor theory of the neocortex. *Nature neuroscience* 27, 7 (2024), 1221–1235.

- [92] RAO, R. P., AND BALLARD, D. H. Predictive coding in the visual cortex: a functional interpretation of some extra-classical receptive-field effects. *Nature Neuroscience* (1999).
- [93] RAO, R. P., GKLEZAKOS, D. C., AND SATHISH, V. Active predictive coding: A unifying neural model for active perception, compositional learning, and hierarchical planning. *Neural Computation* 36, 1 (2023), 1–32.
- [94] RAO, R. P. N. An optimal estimation approach to visual perception and learning. *Vision Research* 39, 11 (1999), 1963–1989.
- [95] RAYNER, K., INHOFF, A. W., MORRISON, R. E., SLOWIACZEK, M. L., AND BERTERA, J. H. Masking of foveal and parafoveal vision during eye fixations in reading. *Journal of Experimental Psychology: Human perception and performance* 7, 1 (1981), 167.
- [96] RENSINK, R. A. The dynamic representation of scenes. *Visual cognition* 7, 1-3 (2000), 17–42.
- [97] RICHEMOND, P. H., GRILL, J.-B., ALTCHÉ, F., TALLEC, C., STRUB, F., BROCK, A., SMITH, S., DE, S., PASCANU, R., PIOT, B., ET AL. Byol works even without batch statistics. *arXiv preprint arXiv:2010.10241* (2020).
- [98] ROBINSON, D. A. The mechanics of human smooth pursuit eye movement. *The Journal of Physiology* 180, 3 (1965), 569.
- [99] ROTHKOPF, C. A., BALLARD, D. H., AND HAYHOE, M. M. Task and context determine where you look. *Journal of vision* 7, 14 (2007), 16–16.
- [100] SALVATORI, T., MALI, A., BUCKLEY, C. L., LUKASIEWICZ, T., RAO, R. P., FRISTON, K., AND ORORBIA, A. Brain-inspired computational intelligence via predictive coding. *arXiv preprint arXiv:2308.07870* (2023).
- [101] SALVATORI, T., PINCHETTI, L., MILLIDGE, B., SONG, Y., BAO, T., BOGACZ, R., AND LUKASIEWICZ, T. Learning on arbitrary graph topologies via predictive coding. *Advances in neural information processing systems* 35 (2022), 38232–38244.
- [102] SALVATORI, T., SONG, Y., HONG, Y., SHA, L., FRIEDER, S., XU, Z., BOGACZ, R., AND LUKASIEWICZ, T. Associative memories via predictive coding. *Advances in Neural Information Processing Systems* 34 (2021), 3874–3886.
- [103] SANOCKI, T. Representation and perception of scenic layout. *Cognitive Psychology* 47, 1 (2003), 43–86.
- [104] SASAKI, Y., HADJIKHANI, N., FISCHL, B., LIU, A. K., MARRET, S., DALE, A. M., AND TOOTELL, R. B. Local and global attention are mapped retinotopically in human occipital cortex. *Proceedings of the National Academy of Sciences* 98, 4 (2001), 2077–2082.
- [105] SETH, A. K., AND HOHWY, J. Predictive processing as an empirical theory for consciousness science. *Cognitive Neuroscience* 12, 2 (2021), 89–90.
- [106] SHARAFELDIN, A., IMAM, N., AND CHOI, H. Active sensing with predictive coding and uncertainty minimization. *Patterns* (2024).
- [107] SRINIVASAN, M. V., LAUGHLIN, S. B., AND DUBS, A. Predictive coding: a fresh view of inhibition in the retina. *Proceedings of the Royal Society of London. Series B. Biological Sciences* 216, 1205 (1982), 427–459.
- [108] STRASBURGER, H., RENTSCHLER, I., AND JÜTTNER, M. Peripheral vision and pattern recognition: A review. *Journal of vision* 11, 5 (2011), 13–13.
- [109] TANG, M., SALVATORI, T., MILLIDGE, B., SONG, Y., LUKASIEWICZ, T., AND BOGACZ, R. Recurrent predictive coding models for associative memory employing covariance learning. *PLoS computational biology* 19, 4 (2023), e1010719.
- [110] VAN DER MAATEN, L., AND HINTON, G. Visualizing data using t-sne. *Journal of machine learning research* 9, 11 (2008).
- [111] VAN DIEPEN, P. M., WAMPERS, M., AND D’YDEWALLE, G. Functional division of the visual field: Moving masks and moving windows. In *Eye guidance in reading and scene perception*. Elsevier, 1998, pp. 337–355.
- [112] WANG, P., AND COTTRELL, G. W. Central and peripheral vision for scene recognition: A neurocomputational modeling exploration. *Journal of vision* 17, 4 (2017), 9–9.
- [113] WESTHEIMER, G., AND MCKEE, S. P. Visual acuity in the presence of retinal-image motion. *JOSA* 65, 7 (1975), 847–850.

- [114] WHITTINGTON, J. C., AND BOGACZ, R. An approximation of the error backpropagation algorithm in a predictive coding network with local hebbian synaptic plasticity. *Neural computation* 29, 5 (2017), 1229–1262.
- [115] WURTZ, R. H., MCALONAN, K., CAVANAUGH, J., AND BERMAN, R. A. Thalamic pathways for active vision. *Trends in cognitive sciences* 15, 4 (2011), 177–184.
- [116] ZBONTAR, J., JING, L., MISRA, I., LECUN, Y., AND DENY, S. Barlow twins: Self-supervised learning via redundancy reduction. In *International conference on machine learning* (2021), PMLR, pp. 12310–12320.
- [117] ZEKI, S. The ferrier lecture 1995 behind the seen: the functional specialization of the brain in space and time. *Philosophical Transactions of the Royal Society B: Biological Sciences* 360, 1458 (2005), 1145–1183.
- [118] ZEKI, S., AND SHIPP, S. The functional logic of cortical connections. *Nature* 335, 6188 (1988), 311–317.
- [119] ZHANG, L., DU, W., ZHOU, S., WANG, J., AND SHI, J. Inpaint2learn: A self-supervised framework for affordance learning. In *Proceedings of the IEEE/CVF Winter Conference on Applications of Computer Vision* (2022), pp. 2665–2674.
- [120] ZIMMERMANN, R. S., SHARMA, Y., SCHNEIDER, S., BETHGE, M., AND BRENDEL, W. Contrastive learning inverts the data generating process. In *International Conference on Machine Learning* (2021), PMLR, pp. 12979–12990.

Appendix / Supplementary Material

Glimpse Vector Creation: Additional Details

Each glimpse-action pair within a K -length (random/involuntary) saccade trajectory or sequence $\{(\mathbf{g}(0), \mathbf{a}(0)), (\mathbf{g}(1), \mathbf{a}(1)), \dots, (\mathbf{g}(k), \mathbf{a}(k)), \dots, (\mathbf{g}(K), \mathbf{a}(K))\}$ is created by first generating a 2D vector contain Cartesian x-y coordinates (in this work, a random policy is used to select each set of coordinates at each step within the trajectory), extracting the relevant glimpse vector $\mathbf{g}(k)$ containing the foveal/parafoveal/peripheral patches at the chosen coordinates, and then finally normalizing the coordinate vector to create the requisite action vector $\mathbf{a}(k)$. Specifically, the 2D x-y coordinate action vector is created by normalizing the original raw x-y Cartesian coordinates to the range of $[-1, 1]$, i.e., $\mathbf{a}(k) = 2\left(\frac{[x, y]^T}{D} - 1\right)$ for a $D \times D$ pixel image where x and y are the original Cartesian coordinates of the glimpse center-point.

Each glimpse vector $\mathbf{g}(k)$ itself is a concatenation of several views (pixel patches) sampled from the observation $\mathbf{o}(t_g)$. Specifically, it is a combination of several types of views, each of which can be expressed in terms of the following piecewise function:

$$\mathbf{p}^v = \begin{cases} \mathbf{p}_c^v \in \mathbb{R}^{S_c \times S_c} & v \in \{\text{Set of foveal patch indices}\} \\ \mathbf{p}_f^v \in \mathbb{R}^{S_f \times S_f} & v \in \{\text{Set of parafoveal patch indices}\} \\ \mathbf{p}_p^v \in \mathbb{R}^{S_p \times S_p} & v \in \{\text{Set of peripheral patch indices}\} \\ \emptyset & \text{otherwise.} \end{cases} \quad (15)$$

To produce the final glimpse vector, all C foveal, F parafoveal, and P peripheral views (centered around the glimpse/gaze’s center-point) are first average pooled to always be the same final shape of $S \times S$ pixels, then flattened to vectors, and finally concatenated to obtain $\mathbf{g}(k) \in \mathbb{R}^{((C+F+P)*(S*S)) \times 1}$. All of the above means that the final glimpse vector produced as a result of the k -th saccade is:

$$\mathbf{g}(k) = \langle \mathbf{g}^1(k), \mathbf{g}^2(k), \dots, \mathbf{g}^v(k), \dots, \mathbf{g}^V(k) \rangle^T \quad (16)$$

where $V = C + F + P$, brackets $\langle \cdot \rangle$ denote vector concatenation, and $\mathbf{g}^v(k) = \text{Flat}(\text{Pool}(\mathbf{p}^v))$. For the main model used in the paper, the set of foveal patch indices was $\{1, 2, 3, 4\}$ while the set of parafoveal indices was $\{5\}$ and the peripheral was $\{6\}$. This choice was made based on preliminary experimentation (the stream configuration that resulted in the best performing MPC model was chosen), the results of which are presented in the next appendix section.

Upon creation, the foveal, parafoveal, and peripheral views are all aligned around a glimpse center-point (the x-y coordinates of the center-point of our model’s gaze) with all views arranged around the center-point in a particular topology (such as a grid). Foveal views are generally shaped such that $S_C = S$ whereas parafoveal views are shaped such that $S_C > S$ and peripheral views are shaped such that $S_P > S_C > S$; in this work, we specifically choose for foveal views $S = S_C = 8$ pixels, for parafoveal views $S_F = 16$ pixels, and for peripheral views $S_P = 24$ pixels. As mentioned above, we use $C = 4$ foveal views which are arranged in a 2×2 grid (such that the foveal views overlap with one another by 1-2 pixels) centered around the whole glimpse/gaze center-point; we only use one ($F = 1$) parafoveal view and one ($P = 1$) peripheral views, which are both directly centered around the glimpse/gaze center-point.

Analysis of View Extraction Schemes

In this supplementary section, we provide some experimental results for a small set of configurations of the input stream patch extraction scheme that we utilize for the MPC and GPC-fov models. Table 2 presents the results of these particular experimental results. Concretely, under each particular configuration of the input stream, we fit an MPC to the training data as in the main paper, then probe the quality of the embeddings with: **1)** a linear probe/classifier, **2)** a nonlinear attentive probe/classifier (set up in the same way as in [18]), and **3)** a nonlinear MLP decoder (for input reconstruction). The training details for the linear probe and MLP decoder are the same as described in the main paper; the nonlinear attention probe was trained under similar conditions to the linear probe (except it was trained using the Adam optimizer, used drop-out for regularization, and employed a decaying adaptive learning rate).

Specifically, we analyze the performance of an MPC model on MNIST under a small set of several possible stream configurations; concretely, we investigate the value of having only one coarser grained view (i.e., just the peripheral) or two (i.e., the parafoveal patch and the peripheral patch) as well as having only a single foveal or multiple (two or four foveal patches). As a result, the input stream configurations that we preliminarily investigated included the following:

F-PF-P	Lin-ACC (%)	Attn-ACC (%)	Dec-MSE (nats)
$C = 1$	96.20 ± 0.07	98.00 ± 0.03	9.283 ± 0.137
$C = 2$	96.40 ± 0.08	98.30 ± 0.08	10.869 ± 0.933
$C = 4$	97.81 ± 0.05	98.80 ± 0.05	5.761 ± 1.222
F-P	Lin-ACC (%)	Attn-ACC (%)	Dec-MSE (nats)
$C = 1$	95.08 ± 0.06	97.71 ± 0.03	9.942 ± 0.763
$C = 2$	96.66 ± 0.04	98.25 ± 0.02	7.481 ± 0.889
$C = 4$	97.56 ± 0.05	98.68 ± 0.04	4.971 ± 0.616

Table 2: **Generalization on MNIST of meta-representational predictive coding under different glimpsing structures.** We examine MPC generalization ability under different formulations of its sensory input stream structure – ‘F-PF-P’ denotes foveal-parafoveal-peripheral whereas ‘F-P’ denotes foveal-peripheral; $C = \{1, 2, 4\}$ controls the amount of foveal streams arranged for the structure (while only one parafoveal or peripheral view are used). We specifically measure generalization in terms of downstream classification ability (in terms of %), as measured by a linear probe (Lin-ACC) and a nonlinear attentive probe (Attn-ACC), as well as downstream decoding ability in terms of mean squared error (Dec-MSE, in terms of nats).

- **Foveal, parafoveal, peripheral (F-PF-P):**
 - One foveal ($C = 1$) + parafoveal + peripheral
 - Two foveal ($C = 2$) + parafoveal + peripheral
 - Four foveal ($C = 4$) + parafoveal + peripheral
- **Foveal and only peripheral (F-P):**
 - One foveal ($C = 1$) + peripheral
 - Two foveal ($C = 2$) + peripheral
 - Four foveal ($C = 4$) + peripheral

In Table 2, we observe that the best classification performance (in terms of both the linear and nonlinear attentive probes) is obtained with $C = 4$, $F = 1$, and $P = 1$; however, slightly better reconstruction comes from just $C = 4$ and $P = 1$ (no parafoveal; $F = 0$). It is important to note that more foveal streams resulted in improved performance in either of these overall settings (with $C = 4$ giving the best in the set of configurations explored). It would prove beneficial if future work were to explore other configurations of the input streams (including both the quantity as well as the spatial arrangement).